CLIMATE PROXIES FROM THE SIWALIK GROUP IN THE EASTERN HIMALAYA: AN OXYGEN AND HYDROGEN ISOTOPE RECORD FROM AUTHIGENIC CLAYS

Beth Cowan

Submitted in Partial Fulfillment of the Requirements for the
Degree of Combined Honours Bachelor of Science,
Department of Oceanography & Department of Earth Sciences

at

Dalhousie University
Halifax, Nova Scotia
April, 2012

Distribution License

DalSpace requires agreement to this non-exclusive distribution license before your item can appear on DalSpace.

NON-EXCLUSIVE DISTRIBUTION LICENSE

You (the author(s) or copyright owner) grant to Dalhousie University the non-exclusive right to reproduce and distribute your submission worldwide in any medium.

You agree that Dalhousie University may, without changing the content, reformat the submission for the purpose of preservation.

You also agree that Dalhousie University may keep more than one copy of this submission for purposes of security, back-up and preservation.

You agree that the submission is your original work, and that you have the right to grant the rights contained in this license. You also agree that your submission does not, to the best of your knowledge, infringe upon anyone's copyright.

If the submission contains material for which you do not hold copyright, you agree that you have obtained the unrestricted permission of the copyright owner to grant Dalhousie University the rights required by this license, and that such third-party owned material is clearly identified and acknowledged within the text or content of the submission.

If the submission is based upon work that has been sponsored or supported by an agency or organization other than Dalhousie University, you assert that you have fulfilled any right of review or other obligations required by such contract or agreement.

Dalhousie University will clearly identify your name(s) as the author(s) or owner(s) of the submission, and will not make any alteration to the content of the files that you have submitted.

If you have questions regarding this license please contact the repository manager at dalspace@dal.ca.

Grant the distribution license by signing and dating below.

_____ _____

Name of signatory Date

TABLE OF CONTENTS

LIST OF FIGURES

LIST OF TABLES

ABSTRACT

There are growing lines of evidence for spatial and temporal correlations between rates of precipitation, surface erosion and deformation along active orogens, however field evidence for couplings and feedbacks between erosional, climatic and tectonic processes are still lacking. The coupled Himalayan orogen and Indian Summer Monsoon (ISM) is an ideal system for the study of these relationships. The Siwalik Group, at the toe of the Himalaya, was formed during the Miocene as the foreland sediment of the uplifting Himalaya. Himalayan orogen is the result of the collision and ongoing convergence of India and Eurasia since ~ 55 Ma. The ISM was established by approximately 12 Ma, as a moist air package moving northward from the Bay of Bengal up to the orographic barrier, formed by the Himalayan foothills, where it rose and cooled, causing a band of high precipitation along the orogenic front. The ISM is perturbed in the eastern Himalaya where the Shillong Plateau, an ~1600 m-high orographic barrier, is located along the northward pathway of the monsoonal circulation, causing high amounts of precipitation along its southern slope and creating a rain shadow in the Bhutan Himalaya to the north.

The uplift of the Shillong Plateau occurred at the Miocene-Pliocene transition, 6-7 Ma, therefore after the ISM had been established and potentially induced a drastic reduction in rainfall along the Bhutan Himalaya front. Meanwhile, low-temperature thermochronological data suggest that the cooling rates (i.e. erosion rates) slowed in Bhutan at the Miocene-Pliocene transition, while the plate convergence rates remained nearly constant, suggesting a temporal correlation between erosion and rainfall distribution.

Since the Siwaliks cover the period of the uplift of the Shillong Plateau, these sediments may carry information on the changes in precipitation patterns and the concomitant changes in erosion in the hinterland. In this study I focus on extracting the climate proxies from the Siwalik sediments to assess the regional climatic changes potentially induced by the uplift of the Shillong Plateau.

A river section in southeastern Bhutan offers ~ 2200 meters of continuous stratigraphic outcrop of the Siwaliks. In this study, measurements of oxygen and hydrogen isotopes in authigenic clays were used to estimate the precipitation within the Himalayan foreland basin at the time of the Shillong Plateau's uplift. Processes of evaporation, condensation, and rain-out of water from air masses passing over mountain belts will systematically affect the isotope composition of the precipitation and therefore of hydrous minerals formed by weathering. Isotopic results show an overall increase in $\delta^{18}O$ from the Siwalik deposition to Recent. Since the Miocene there has been a general cooling trend as global ice volume has increased, which has also affected the Bhutan Himalaya through the weakening of the ISM since 2.7 Ma. This trend accounts for some of the isotopic change, but not all that has been observed in this study. Therefore the uplift of the Shillong Plateau is the most viable cause for the change in precipitation distribution since the Siwalik deposition. These results are the first continental paleoclimatic record for the eastern Himalaya, indicating higher precipitation within the foreland basin of eastern Bhutan during the deposition of the Siwalik Group. Accurate dating of the sediments (magnetostratigraphy, detrital thermochronology) will allow us to compare our isotopic data with the established marine record and provide a final interpretation.

Keywords: Himalayan orogen, foreland sediments, monsoon, paleoclimate, continental record

LIST OF ABBREVIATIONS

MHT	Main Himalayan Thrust
MBT	Main Boundary Thrust
MFT	Main Frontal Thrust
MCT	Main Central Thrust
LHS	Lesser Himalaya Sequence
ISM	Indian Summer Monsoon
XRD	X-Ray Diffraction
VSMOW	Vienna Standard Mean Ocean Water
GMWL	Global Meteoric Water Line
LMWL	Local Meteoric Water Line

ACKNOWLEDGEMENTS

I would like to extend my sincerest gratitude to my supervisor, Dr. Djordje Grujic, for providing me with the opportunity to work on both a challenging and rewarding project, for inspiring my fascination in the subject and Bhutan, and for allowing me to venture to Switzerland, with help every step of the way. It was a pleasure to work with someone so wholly motivated and fascinated by his work.

Thank you to Dr. Isabelle Coutand for all her work in the field, and for helping me to understand the geology of Bhutan, as well as for her guidance and support throughout the research. I would also like to thank Dr. Martin Gibling for his help with the writing process throughout the year and for stretching my mind through the final hurdles.

Thanks to the many lab technicians and students working in the labs that taught me new techniques and kept me entertained and motivated through my analyses. I would like to thank the following Dalhousie technicians: Keith Taylor, Guang Yang, and Matt Kliffer. I would also like to thank Torsten Vennemann and Kerstin Bauer from the University of Lausanne for housing me, for teaching me to master the ways of mass spectrometry and for guiding me through my time in Switzerland.

CHAPTER I: INTRODUCTION

1.1 INTRODUCTION

The Siwalik Group of the Subhimalaya has been the focus of several sedimentological, structural, and chronostratigraphic studies due to its potential for yielding the tectonic and erosional histories of the Himalaya (Ojha et al., 2000; Najman 2006; Bernet et al., 2010). The erosional constraints of the Himalaya are controlled by the Indian Summer Monsoon (ISM), which has created some of the wettest regions on Earth and has been present for at least 12 Ma (Dettman et al., 2003) and up to 24 Ma (Clift et al., 2008). To date, research on Siwalik sediments predominantly has been conducted on the western and central Himalaya, with little from the east. Local paleoclimate studies have been conducted on western Himalaya sediments, with regional studies of the Arabian Sea and Indian Ocean marine sediments (Clemens et al., 1991; Overpeck et al., 1996). However a continental paleoclimate record of the eastern Himalaya has not been documented. This segment of the Himalaya is of a particular interest because it may have been affected by a geologically recent and significant change in mean precipitation rate. Namely, eastern Bhutan is located directly north of the Shillong Plateau, the 1600 m- high orographic barrier to the northward circulation of the ISM. Precipitation can reach >12 m/year at the southern flank of the Shillong Plateau (Bookhagen et al., 2010). The understanding of paleoclimate variation of eastern Bhutan could lead to further knowledge about the timing of the uplift of the Shillong Plateau as well as the understanding of rain shadow formation and the feedback between precipitation (i.e. climate), erosion and tectonics.

The research for this study has the following objectives: (a) to quantify the climatic pattern over the course of the Siwalik deposition, Middle Miocene-Middle Pliocene; (b) to determine the regional and local climatic patterns; and (c) to discern whether the Siwalik sediments can provide evidence of the uplift of the Shillong Plateau and its impact on the climate patterns of eastern Bhutan. To achieve these objectives, 87 paleosol samples were taken along a river transect in southeastern Bhutan (Fig. 1.1). I cleaned and separated the samples to obtain the

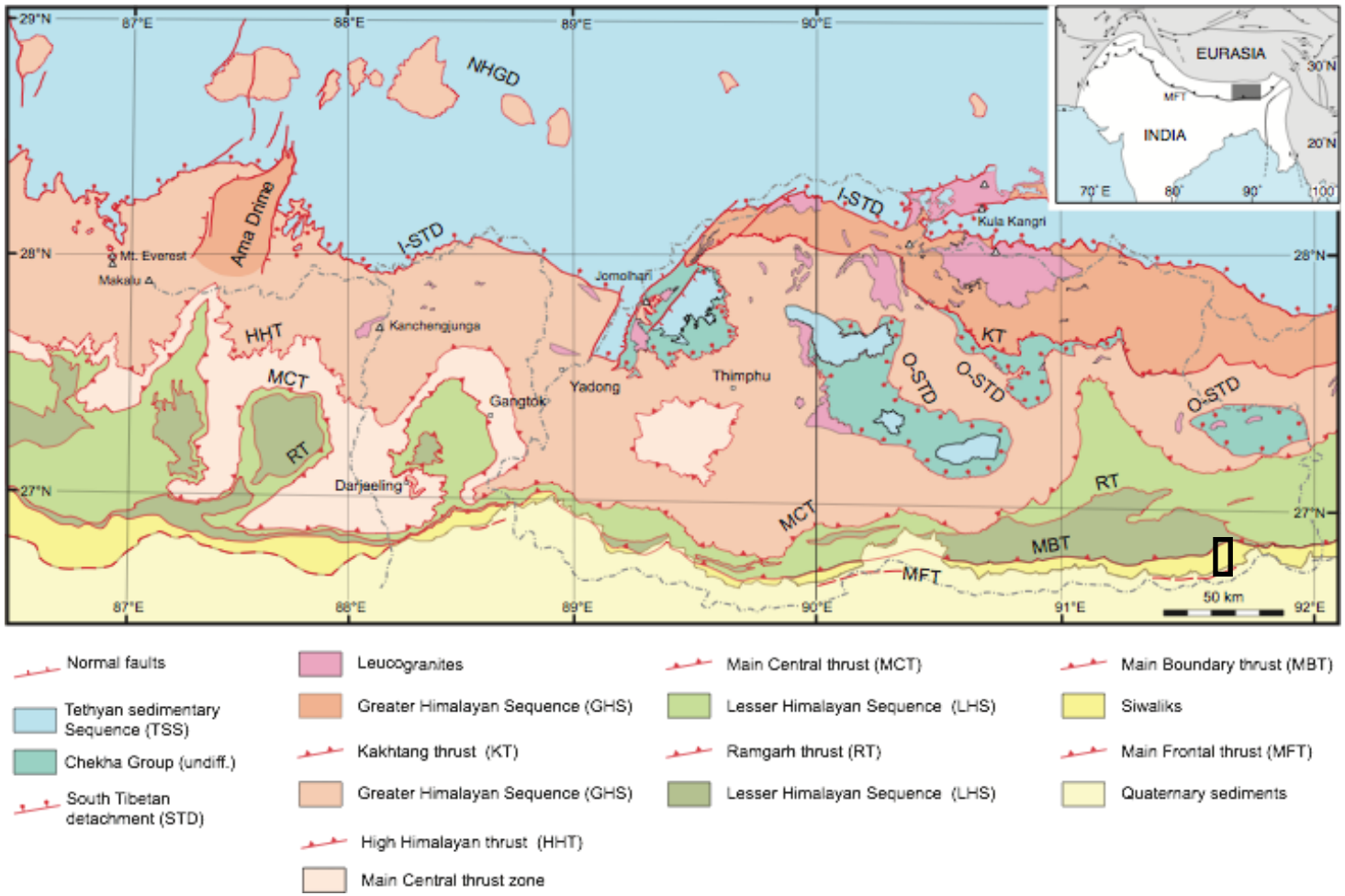

Figure 1.1: Simplified geological map of Bhutan, Sikkim and Eastern Nepal (from Grujic et al., 2011). With inset showing its location within the Himalaya-Tibet orogen. O-STD-, I ST-D outer and inner South Tibetan detachment, respectively: HHT—High Himalayan Thrust; MBT—Main Boundary thrust; MCT—Main Central thrust; MFT—Main Frontal thrust; KT—Kakhtang thrust; RT—Ramgarh thrust; LF—Lingshi fault; YF—Yadong fault, NHGD—North Himalayan gneiss domes. The highlighted black box indicates the location of the Samdrup Jongkhar transect across the Siwaliks in the SE Bhutan.

clay grain size fraction which I characterized using X-ray diffraction (XRD), and analyzed for oxygen and hydrogen isotopes.

1.2 MONSOON AND PALEOCLIMATE OF THE REGION

The Indian Summer Monsoon (ISM) has created some of the wettest regions on Earth, and has had fundamental effects on the climate of South Asia (Fig. 1.2). The ISM is driven by the heating of the Tibetan Plateau in April and May creating a region of low pressure (Dettman et al., 2001). Consequently, the warm moist air from the Indian Ocean is pulled inland by the low pressure region, creating southwesterly winds. As the moist warm air moves across the Indian subcontinent it eventually hits an orographic barrier, the Himalaya, which forces the air mass upwards where it cools, condenses and forms precipitation. The ISM propagates northwest along the Himalaya front, where Bhutan receives the monsoonal precipitation in the first week of June before it continues along the Himalaya (Bookhagen et al., 2006, 2010).

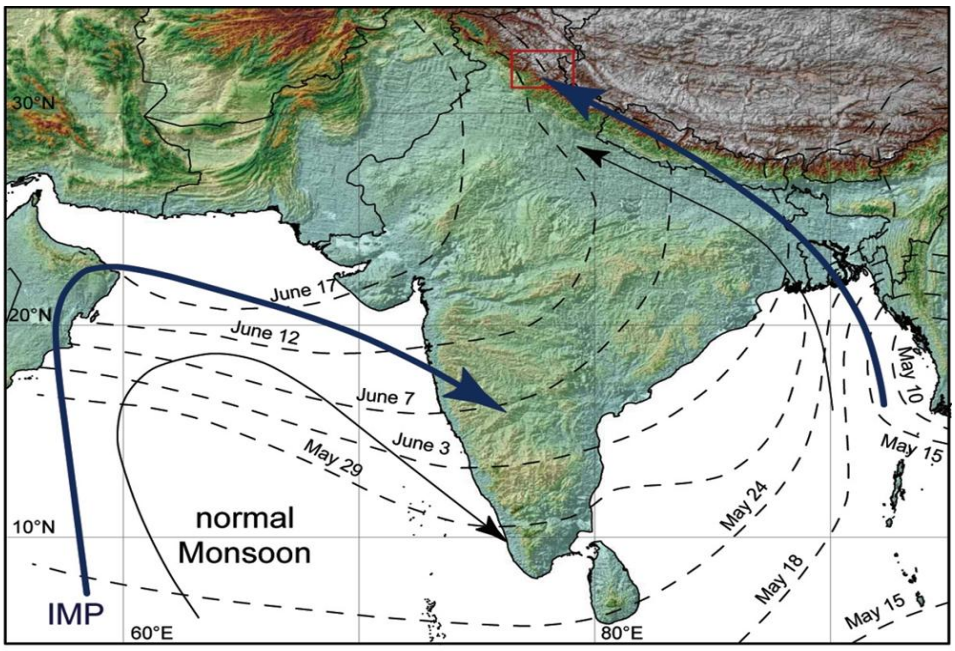

Figure 1.2: The present propagation (arrows) of the Indian Summer Monsoon (ISM) with isoclines for the date at which the monsoon reaches a region. From Bookhagen et al. (2005).

The onset of the monsoon in geological time is unclear, and is a topic of continuous debate. Quade et al. (1995) found that the marine record in the northern Indian Ocean shows evidence from diatom assemblages for the monsoon circulation to have appeared by 11-10 Ma. Oxygen isotopes of fossil bivalves and mammal teeth from the Middle Siwalik sections within Nepal indicate that there has been strong wet-dry seasonality throughout the past 11 Ma (Dettman et al., 2001). The reorganization of environmental belts in China along with alternating layers of eolian dust and soils in the Chinese loess plateau, from stronger to weaker monsoon cycles, suggest the monsoon to have been established at the beginning of the Neogene, ~ 24 Ma (Clift et al., 2008).

A major change in the climate of the Himalaya foreland basin occurred approximately at 7-8 Ma. This is shown in the geological record as the dramatic shift of forest biomass to C3 and C4 (grassland) biomass beginning ~7-7.4 Ma (Quade et al., 1989). Oxygen isotopes also show evidence of this shift towards a wetter climate during the Late Miocene. Quade et al. (1989) attributed this shift to an intensification of the monsoon, with the introduction of C4 biomass that is favoured by the summer monsoonal climate. Marine diatom assemblages from the Bay of Bengal also record the onset and the intensification of the monsoon, and increased remarkably at 7.3 Ma with the intensification of the monsoon (Quade et al., 1989; Dettman et al., 2001).

Pollen, foraminifera and $\delta^{13}C$ analysis from north-west India, northern Indian Ocean and the Arabian Sea indicate global Pleistocene cooling that started at 2.7 Ma, which marked a dry and semiarid climate regime and a weak monsoon for the Himalayas while the middle latitudes experienced increased ice volumes during the last glacial maximum (Thomas et al., 2002). The cooler and drier climate resulted in less developed yellow paleosols with slower pedogenesis. At 0.9 Ma further aridification occurred, changing the depositional system from braided streams to gravity flows in the Piedmont system along the Himalaya front (Thomas et al., 2002).

1.3 SHILLONG PLATEAU

In eastern Bhutan is the only segment of the Himalayan range situated adjacent to the uplifted basement rocks of the Peninsular India, in the form of the Shillong Plateau (Gansser, 1983). It is the only orographic barrier present within the Himalayan foreland. The Shillong Plateau lies directly within the northward trajectory of the ISM, such that it changes the regional distribution of precipitation away from the Himalayan front (Bookhagen et al., 2010). The plateau presents a 1600 m-high orographic barrier to the prevailing winds from the Bay of Bengal that transports moist air northwards towards the Himalaya front. It is suggested that the plateau has reduced the mean annual precipitation in the downwind eastern Bhutan Himalaya front (Fig. 1.3; Grujic et al., 2006; Biswas et al., 2007; Bookhagen et al., 2010). This extraction of precipitation away from the Himalaya front is suggested to have begun with the uplift of the Shillong Plateau at the Miocene-Pliocene transition (Grujic et al., 2006; Clark et al., 2008).

At present the Shillong Plateau concentrates rainfall at its southern slope with approximately 11,000 mm/yr (Breitenbach et al., 2010), creating a rain-shadow to the north on its leeward side (Grujic et al., 2006; Bookhagen et al., 2010) with a mean annual precipitation rate of 5300 mm/yr at Samdrup Jongkhar (Royal Government of Bhutan, 2012).

The Shillong Plateau is an outcrop of Precambrian basement rock that was covered by Tertiary shallow marine and deltaic sediments. Late Cretaceous continental sediments lie unconformably upon the basement bedrock indicating surface exposure of the bedrock during the Cretaceous which is also suggested by thermochronological data (Biswas et al., 2007). The basement was buried until the Miocene-Pliocene transition and covered by up to 3000-6000 m of shallow marine and deltaic sediments, indicating a depositional environment at the passive margin of the Indian plate (Biswas et al. 2007). The rock uplift of the Shillong Plateau started exhumation between 15.2-8.9 Ma as indicated by apatite (U-Th-[Sm])/He and apatite fission track data (Biswas et al., 2007). The soft Tertiary sediments were eroded quickly, and as a consequence the rock uplift did

not result in a significant surface uplift, such that once the bedrock was uncovered (at the Miocene-Pliocene transition) the erosion rate decreased resulting in surface uplift. The slip along the faults bounding the Shillong Plateau may account for up to one-third of the India-Eurasia convergence (Biswas et al., 2007). The cause of the Shillong Plateau uplift is not yet clear. Biswas et al. (2007) interpreted the plateau to have formed as a result of the contractional deformation during the Indo-Eurasian collision, as a combination of reactivation (i.e. inversion) of the passive margin normal faults and crustal tilting. Clark et al. (2008) interpreted the Shillong Plateau deformation to be coincident with major changes in regional strain patterns within the southern Tibetan Plateau and along its eastern margin. Bilham et al. (2003) interpreted the Shillong Plateau as a basement pop-up structure caused primarily by the crustal bending resulting from the sediment load in the Bengal fan.

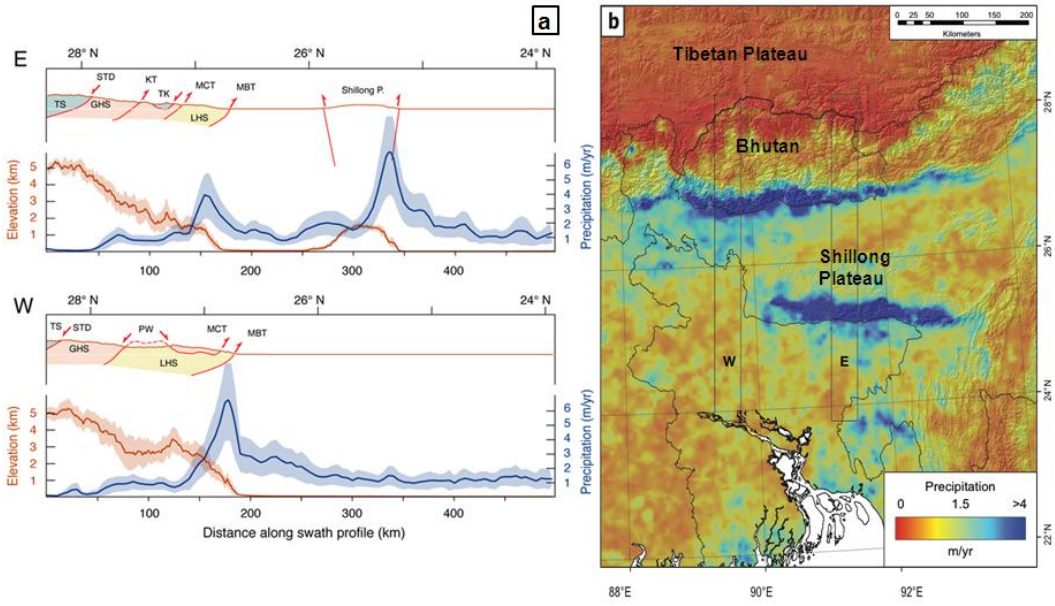

Figure 1.3: a) Topographic and precipitation profiles across Bhutan Himalayas and Shillong Plateau to the south (from Grujic et al., 2006). The Shillong plateau acts as an 1.5-2 km orographic barrier to hinder moisture transport from the Bay of Bengal to the Himalayan front, strongly affecting the site of the Indian Summer Monsoon (ISM) precipitation. E: eastern Bhutan; W: western Bhutan. Precipitation (blue) data were derived from the calibrated Tropical Rainfall Measuring Mission data, and the topography (orange) data were taken from the Shuttle Radar Topography Mission data. b) Geographic locations for (a), present day thematic map of precipitation distribution, where the Shillong plateau is situated at the southern precipitation maximum. Note the distribution of precipitation: minimal precipitation at the eastern Bhutan border with the Shillong plateau to the south, compared to the west with maximum precipitation at the Himalayan front. From Grujic et al. (2006).

From the placement of the Shillong Plateau, and from the difference in precipitation distribution between eastern and western Bhutan, this study hypothesized that the precipitation distribution along the eastern Himalaya changed with the uplift of the Shillong Plateau at the Miocene-Pliocene boundary. Such that, the precipitation levels in eastern Bhutan have decreased since the uplift of the Shillong Plateau.

CHAPTER II: GEOLOGICAL BACKGROUND

2.1 HIMALAYAN TECTONICS

The Himalayan-Tibetan orogen is the result of the collision of the Indian and Eurasian plates, after the closure of the Tethyan Ocean, at approximately 60-55 Ma. It is regarded as the leading example of a large-scale continental collisional orogeny (Fig. 2.1a; Quade et al., 1995; Hodges et al., 1996). The southern flank of the orogen, the Himalaya, is predominantly a south-propagating fold and thrust system (Fig. 2.1b; Kellett, 2010). This fold and thrust system is made up of rocks that were originally deposited upon India's northern margin. The southward propagating thrusts are rooted into a common basal detachment, the Main Himalayan Thrust (MHT) which bounds the Himalayan orogen to the south and makes up the two thrusts that bound the Subhimalayan rock unit: the youngest and southernmost thrust, the Main Frontal Thrust (MFT) and the Main Boundary Thrust (MBT) to the north (Kellett, 2010). The Lesser Himalayan Sequence was thrust upon the Subhimalaya Formation by the MBT to the south, and is bounded to the north by the Miocene-age Main Central Thrust (MCT). The Subhimalaya Formation is made up of the Siwalik Group, which was deposited with the Lesser Himalaya sequence within the foreland basin of the Himalaya orogen as part of the continental collision. The sediments that were eroded from the orogen were deposited within a basin formed between the mountains and the flexural bulge further south, situated parallel to the foreland basin in NE India approximately 600 km away from the Himalaya front (Biswas et al., 2007). This bulge was formed as an elastic response to the flexural bending of the Indian plate due to the collision and underthrusting beneath the Himalaya and southern Tibet (Beaumont, 1981). As the Himalaya orogen advanced so did the bulge and foreland basin between, causing an evolution of tectonic sediment deposition with the advancing active basin, moving from muddy floodplain to sand to gravel deposition along a stratigraphic section (Parkash et al., 1980).

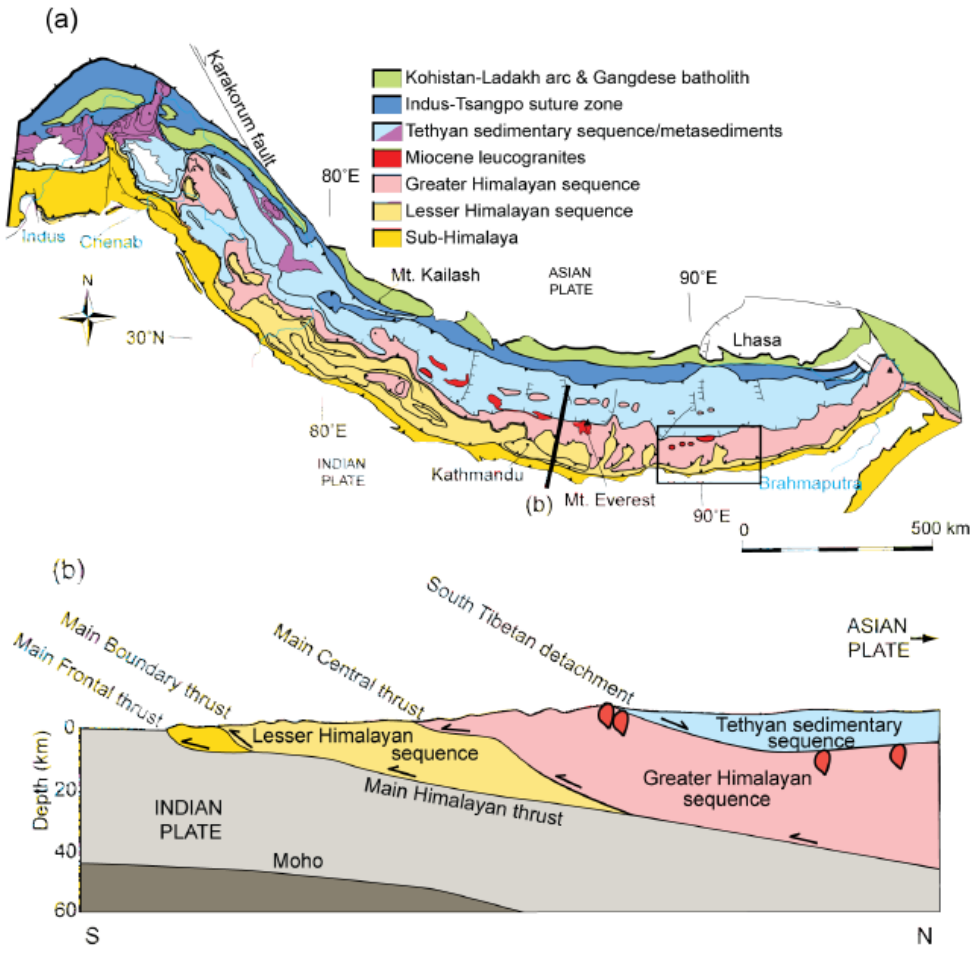

Figure 2.1: a) Geological map of the Himalayan orogen including the main lithotectonic units and structures. **b)** Representative schematic cross-section of the Himalaya through central Nepal, to the south is the foreland and to the north is the Tibetan Plateau. From Kellett, (2010).

2.1.1 MAIN BOUNDARY THRUST

The Main Boundary Thrust (MBT) is the floor thrust of the Lesser Himalaya thrust system, truncating the Subhimalaya Formation to the north by placing Lesser Himalaya Sequence (LHS) sediments of pre-Tertiary age over the un-metamorphosed clastic Siwalik Group of the Himalaya foreland basin (Quade et al., 1995; Huyghe et al., 2001). The initial slip of the MBT is attributed to the doubling of the sediment accumulation rate along sections from northern Pakistan to northern India, enhancing the loading of sediment in the foreland basin (Ojha et al., 2009). From this interpretation by Meigs et al. (1995) and Burbank et al. (1996), the initial movement of the MBT started at approximately

11 Ma. The thrust would have propagated from western to eastern Nepal, approximately 600 km, over 5.8 Myr, which would result in a rate of 103 mm/yr (Ojha et al., 2009). This rate is nearly double the typical rates of lateral propagation within thrust systems of the Himalaya, and instead the MBT is suggested to have occurred as a series of independent, unlinked thrusts that formed the single trace of the MBT (Ojha et al., 2009). Both the MBT and the Main Frontal Thrust (MFT) are thrust fault branches of the Main Himalayan detachment, with regional fault trends beginning in the west and propagating towards the east.

2.1.2 MAIN FRONTAL THRUST

The MFT is the youngest and southernmost active thrust system of the Himalayan orogen that bounds the Siwaliks against the Quaternary alluvial sediments to the south. The MFT became active in Nepal at 2.4-1.8 Ma (Huyghe et al., 2005), at which point the former depositional system within the foreland basin was converted into an area of active erosion (Quade et al., 1995; Huyghe et al., 2005). Active through the Quaternary period, historical seismicity indicates that the MFT is still episodically active, except in western Nepal where it has been locked for approximately 800 years (Jouanne et al., 2004). The MFT may be undergoing a similar tectonic evolution to the MBT; rather than being active simultaneously along a continuous thrust more than 1000 km long, it consists of developing as a series of independent, unlinked local thrusts (Ojha, et al., 2009).

2.1.3 SIWALIK GROUP

The sediments of the Siwalik Group have been studied using many techniques to determine provenance, clay mineralogy, and ages to constrain tectonostratigraphic and paleoclimatic events. Najman (2004) used detrital apatite fission track data from the Siwalik sediments to constrain the final exhumation of the basin sediments, providing a defined date for the start of the continental deposition. Najman (2006) covered a large range of applications for the detrital studies of the Siwalik Group to evaluate tectonic problems. Techniques include petrography, heavy mineral analysis, XRF, and Sr-Nd studies from sediments eroded from the Himalaya orogen and preserved in the foreland

basin, as well as single detrital grain dating by Ar-Ar, U-Pb and fission track methods, Sm-Nd and Pb isotopic analyses. These studies were used to document how the sediment record can be used to determine thermal and tectonic evolution of the orogen, establish exhumation rates, constrain mechanisms of continental deformation, and identify paleodrainage (Najman, 2006). The erosional history of the Himalaya is constrained by sedimentological and Nd isotope data (Huyghe et al., 2001; Bernet et al., 2006).

The Subhimalaya Formation lies gradationally above the Miocene Dharamsala Formation to the south bounded by the MFT (Parkash et al., 1980, Najman 2004). The Sub-Himalaya Formation is made up of the Siwalik Group (Fig. 2.2), a 5000 m thick sequence of clastic sediments that were deposited as a freshwater molasse deposit from Middle Miocene to Late Pliocene (Thomas et al., 2002). Siwalik sediments were deposited synorogenically, in a foreland basin, a forerunner to the Indo-Gangetic Plains (Parkash et al., 1980), which was formed as a consequence of a flexural bulge in the Indian plate resulting from its collision with the Tibetan plate, approximately at 60 Ma (Beaumont, 1981; Bilham et al., 2003; Najman et al., 2004). These sediments record the erosional history of the Himalaya belt along with the paleoclimate of the region during their deposition (Huyghe et al., 2001; Najman, 2006; Bernet, 2010). Fluvial sedimentation acted as the predominant depositional process from 20 Ma through to the present, with recent sedimentation as a continuation of the Siwalik molasse deposit (Thomas et al., 2002). Deposition within the Siwalik Group was dominated by two types of river system, the first being a trunk river system that was mainly braided, and the second being the smaller river systems that formed the tributaries to the trunk river, including both meandering and braided rivers (Thomas et al., 2002). The sedimentation took place as a set of fluvial megafans, with sedimentation rates in Nepal determined to be 0.28 to 0.56 mm/yr increasing with time (Ojha et al., 2009; Bernet, 2010).

Due to the large expanse over which Siwalik sediments were deposited, their characteristics vary along the Himalaya belt, and they have slight differences along each transverse. Although there is no formal nomenclature for

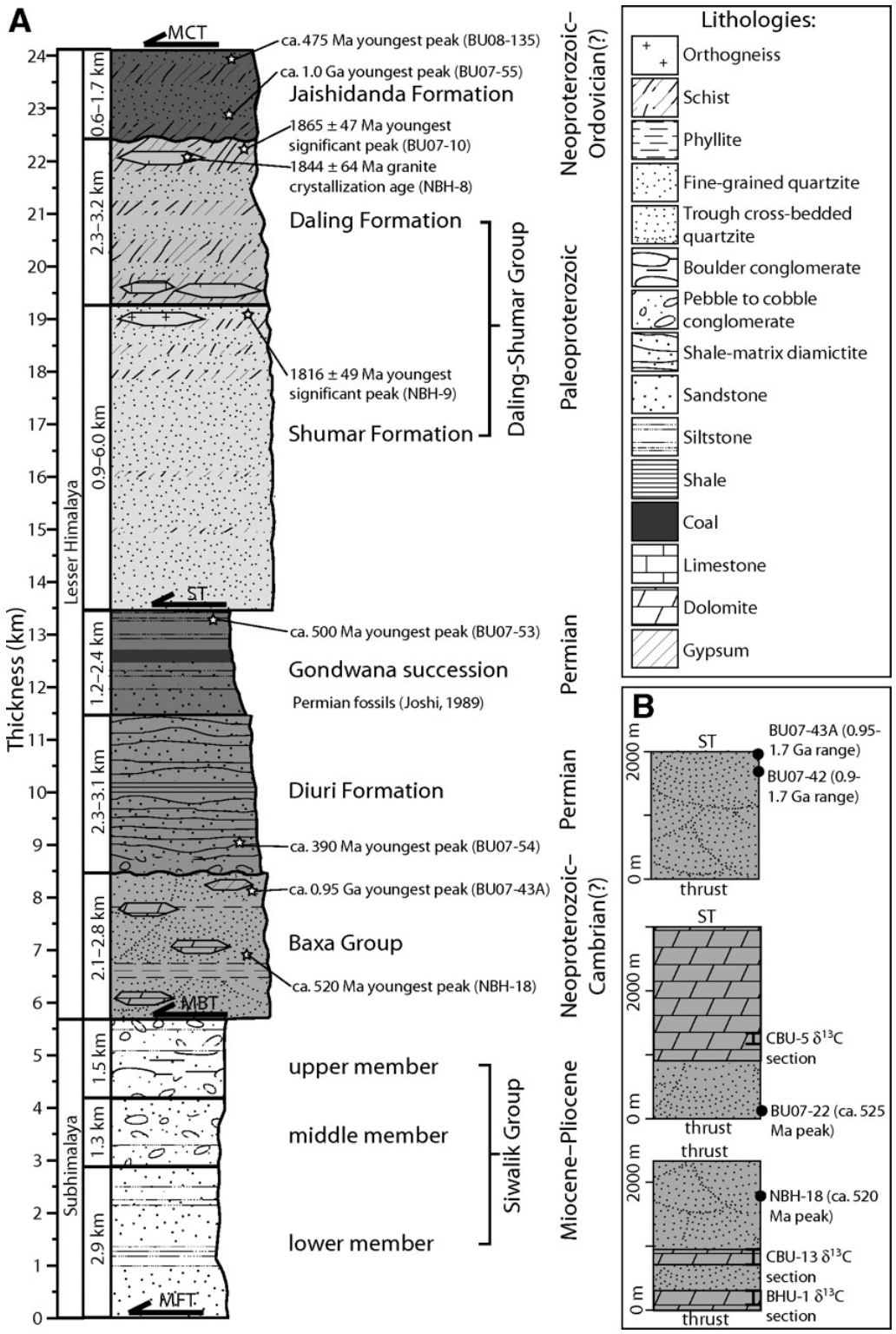

Figure 2.2: Tectonostratigraphy of the Subhimalaya and Lesser Himalaya units of Bhutan depicting the three subgroups of the Siwalik Group within the Subhimalaya. From Long et al. (2011).

the stratigraphy of the Siwalik Group, it has been informally divided into three subgroups: Lower, Middle and Upper Siwalik (Fig. 2.3) (DeCelles et al., 1998). These subgroups have been defined using marked and systematic textural differences (Quade et al., 1995) and heavy mineral assemblages along with lithology, bedding characteristics, degree of induration and texture (Parkash et al., 1980) as well as paleontological records (Najman et al., 2004 & 2006). Overall the Siwaliks are a coarsening upwards sequence made up of a range of mudstones and paleosols coarsening into sandstones and topped by conglomerates (Ojha et al., 2009). Within the coarser Middle to Upper Siwalik lithologies mudstones and paleosols are also present due to seasonal flooding of the depositional rivers. The overall thickness of this sequence was measured with a depth-converted stratigraphic section by Ojha et al., (2009) and varies from 2 to 6 km in Nepal. However, because the Siwalik Group is truncated at its' base and top due to fault sequences, the complete stratigraphic section is rarely exposed.

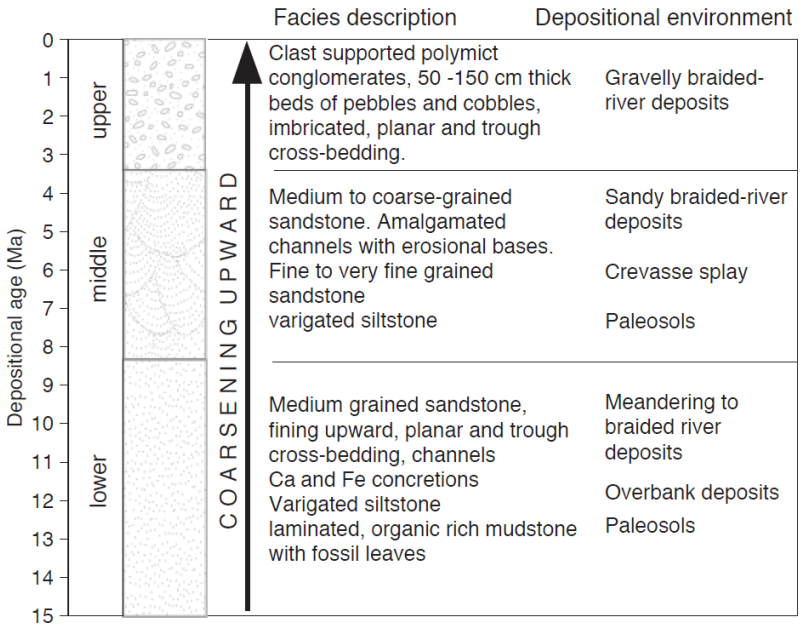

Figure 2.3: A generalized stratigraphic section of the Siwalik Group from western Nepal with short facies descriptions and depositional environment. Modified from Bernet et al. (2006).

The Lower Siwalik is characterized by gray to greenish gray shale interbedded with numerous thick (1-10 m) lenticular channel bodies of fine to medium-grained sandstone, red floodplain siltstones cemented with calcite, and calcareous paleosols with local calcareous nodules in Nepal and Pakistan (Quade et al., 1995; Huyghe et al., 2001; Ojha et al., 2009). The unit is estimated to be approximately 900 m thick in Khutia Khola, Nepal (DeCelles et al., 1998). Sandstone beds increase in thickness in each succeeding cycle, and are characterized by Quade et al. (1995) to be moderately mature lithic arenites with abundant mica. Throughout the subgroup leaf impressions are found, along with low amounts of organics and the occasional coal logs, the succession of carbonaceous shales increase upwards through the section (Quade et al., 1995). Such characteristics provide evidence that large meandering rivers and their expansive floodplains were the dominant form of deposition within the Lower Siwalik landscape. The conformable transition into the Middle Siwalik correlates with a depositional change from meandering rivers into braided river systems (Parkash et al., 1980) due to the evolution of the active foreland basin (DeCelles et al., 1998).

The Middle Siwaliks are dominated by darker gray, greenish gray laminated siltstones with thick multistory (>20 m) channel sandstones bodies, conglomeratic sandstone and lenses of shale (Najman et al., 2004; Ojha et al., 2000, 2009). These rocks are less calcareous and less cemented with an overall thickness of approximately 2400 m in northern Pakistan and Khutia Khola, Nepal (Tripathi, 1986; DeCelles et al., 1998). Channel scour zones are gently wavy with concentrations of reworked clasts increasing in size from the base (10 cm) to the upper section (300 cm). Sedimentary structures within the sandstone beds include tabular and wedge-shaped cross-bedding, small- to large-scale channel scours, and lamination. Leaf impressions are preserved in clay beds, and fossil wood can be found (Quade et al., 1995).

The Upper Siwaliks lie conformably upon the Middle Siwaliks and are dominated by conglomerate (>50%) with a bedding thickness of up to 10 m. The unit is at least 1000 m thick in Khutia Khola, Nepal (DeCelles et al., 1998). The conglomerates are matrix and clast supported, with moderately well to poorly

sorted clasts of quartzite, gneiss and granite, imbricated and interposed with bedded siltstones and yellow paleosols (Quade et al., 1995; Ojha et al, 2000). The depositional environment was dominated by conglomeratic fluvial systems and stream-dominated alluvial fans, with channel features observed locally in the conglomerate (Ojha et al., 2009).

2.1.3.1 DEPOSITIONAL AGE OF THE SIWALIK GROUP

Ojha et al. (2009) have compiled the most complete correlation of the Siwalik Group across the Himalaya belt with both stratigraphy and ages using magnetic polarity and carbon isotope methods (Fig. 2.4). The dated sections of the Siwalik Group range in age from approximately 15 to 1 Ma, with the Lower Siwalik as the oldest unit and the Middle and Upper Siwalik as progressively younger. The major lithostratigraphic boundaries between subgroups of the Siwalik Group were shown to exhibit a 2 Myr diachroneity so that they cannot be simply used to estimate the timing of paleoclimate changes associated with the ISM (Ojha et al., 2009). The ages of the boundaries between subgroups are from 11.5-8 Ma for the Lower to Middle Siwalik, and from 4.5-2 Ma for the Middle to Upper Siwalik boundary.

2.1.3.2 PALEOSOLS

Pedogenic calcite concretion deposits in paleosols have been used to commonly reconstruct paleoclimate, however pedogenic calcite is only found in moderate to low rainfall regions. In paleosols lacking soil-formed calcite, pedogenic non-carbonate minerals can be used for paleoclimate reconstruction (Stern et al., 1997). Pedogenic clay minerals have been found to be a powerful paleoclimate indicator. This is therefore an influential method, since pedogenic clay minerals are far more common in paleosols than pedogenic calcite (Stern et al., 1997).

Overall the paleosols found within the Siwalik Group are bioturbated and in central and western Himalaya have leached red, yellow or greenish horizons, usually enriched in illuvial clays (Quade et al., 1995). Within Nepal, the Lower Siwalik has mostly red and orange paleosols, although paleosols are generally more abundant within the Lower Siwalik, the Middle and Upper Siwalik also

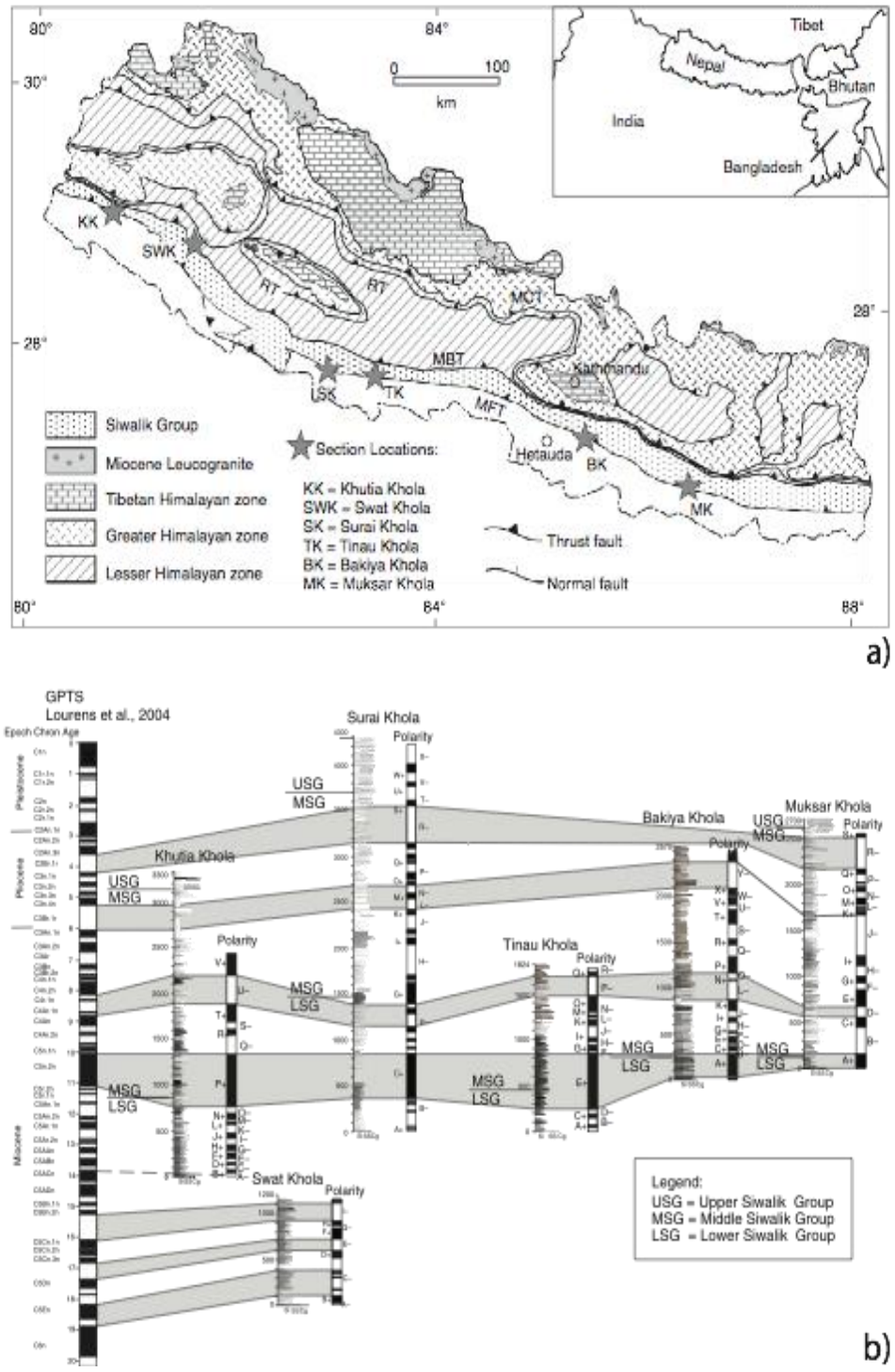

Figure 2.4: a) Regional map across Nepal with site locations for magnetostratigraphy and stratigraphic measurements **b)** The regional correlation from west to east across Nepal from Ojha et al. (2009). The major correlation intervals are highlighted by the grey areas, with the section correlated with chron C5n.2n. This places the boundary between Lower and Middle Siwalik within the range of 11.5-8 Ma, the boundary between Middle and Upper Siwalik within 4.5-2 Ma.

display gray and yellow paleosols (DeCelles et al., 1998). The reddish colour of some units is due to the extent of oxidation, whereas the higher organic contents that lack oxidation result in the grey units. Paleosols are rarely found as isolated facies, but instead are generally 2-40 m thick, consisting of 2-11 units (Thomas et al., 2002). The paleosols within the Siwalik Group have been determined to be pedogenic (i.e. authigenic) at the Potwar Plateau, Pakistan, since the variations of $\delta^{18}O$ values of smectite are synchronous to the $\delta^{18}O$ variations of pedogenic calcite (Stern et al., 1997).

The Siwalik Group provides an integration of fluvial lithofacies and pedofacies, which reflect two different depositional systems similar to those observed in the modern Indo-Gangetic Plains (Thomas et al., 2002). The first is the Lowland System which deposited alluvial megafans with interfan areas, resulting in sand-rich and mud-rich sequences and less developed soils. The second is the Upland System, where large tracks of land remain at higher elevation and therefore receive less sand deposition, thus giving the time and accumulation space for soils to develop. The tilting and uplift of large tectonic blocks are the controlling factors for which system, a Lowland or Upland System, dominates a region (Thomas et al., 2002).

2.1.3.3 EASTERN BHUTAN

The Subhimalaya Formation of eastern Bhutan consists of the Siwalik molasse structurally overlain variously by the Diuri Formation and Baxa Group of the LHS along the MBT to the north and bounded by the Quaternary alluvial deposits of the Brahmaputra Plain to the south along the MFT (Gansser, 1983; Lakshminarayana et al., 1995). The Siwalik is divided into 3 subgroups, all of which are exposed in eastern Bhutan along the Samdrup Jongkhar section, whereas only the Lower and Middle subgroups are well developed west of Bhutan (Fig. 2.5a). The stratigraphy of eastern Bhutan Siwalik is similar to that of the western Himalaya with an overall coarsening upwards succession from interbedded siltstone and shale to massive argillaceous sandstone beds dipping to the north, with pebble to boulder size conglomerates at the top. Each subgroup lies conformably upon the lower unit (Lakshminarayana et al., 1995).

The Samdrup Jongkhar transect was chosen for this study because it is in the lee of the Shillong Plateau and it is the only accessible continuous section with all three Siwalik subgroups exposed (Fig. 2.5a). The transect starts approximately at the MFT, indicated by the progressive southward increase in folding and cleavage development which eventually overprints the sedimentary bedding. In addition to folding between sample locations SB4-2 and SB7-2 (Fig. 2.5b), there is also no continuous outcropping and it is therefore difficult to assess the thickness of the beds. At sample site SB7-2 the continuous section begins, where preliminary facies analysis has determined the sediments to be marine. The Lower Siwalik then begins approximately at sample site SB19-2 (Fig. 2.6).

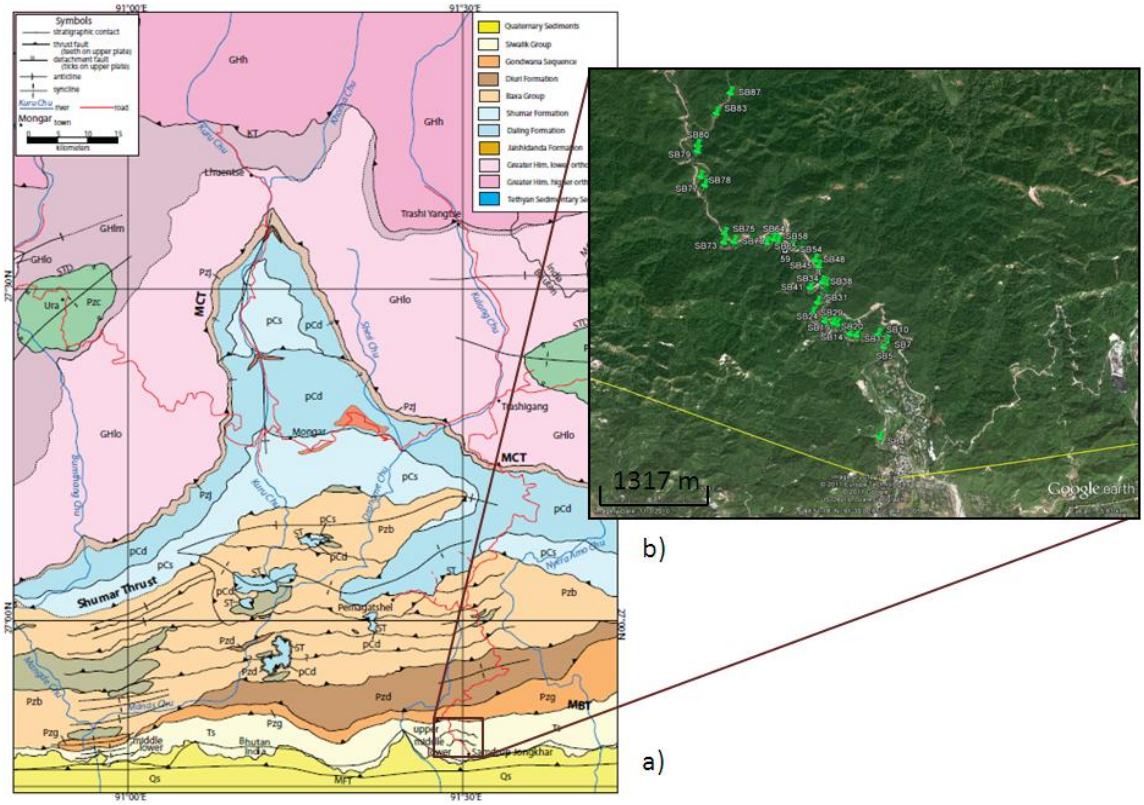

Figure 2.5: a) Geological map of eastern Bhutan with the three subgroups of the Siwaliks and their boundaries along the highlighted Samdrup Jongkhar transect as well across the southern Himalaya front. See the next outcropping to the west, where only the Lower and Middle Siwaliks are found. From Long et al. (2011). **b)** Google Earth image of the Samdrup Jongkhar transect, with sample GPS locations along the river. The yellow line is the Bhutan, India border.

The exposed section of the Lower Siwalik is approximately 425 m thick, and is made up of siltstone, mudstone and fine-grained sandstone (200 m thick) gradually coarsening upwards into thick packages of alternating coarse-grained and medium-grained sandstone. At the upper end of the Lower Siwalik is a change into massive coarse-grained sandstone, ~20 m thick packages, for a total of 325 m. This section reverts back to some interbedding of fine- to medium-grained sandstone layers. The Middle Siwalik transitions conformably from the Lower Siwalik into predominantly coarse-grained sandstone, lacking both the interbedding of finer-grained sandstone and bedding within the massive sandstone beds. In this section bedding is marked by gravel to pebble sized intercallations in channels. Up the section these channel scour deposits become more pebbly, with a matrix of coarse-grained sandstone. The transition to Upper Siwalik is marked by the sudden change into block-sized conglomerates, with occasional coarse-grained sandstone channel scours lined with pebbles. The studied section finishes in the core of an inverted syncline. North of the core the beds are inverted. There is an indication that the Lower Siwalik reappears briefly, suggesting a thrust in the inverted limb of the syncline. Up section the continuity is obstructed, with fewer and more scattered outcrops.

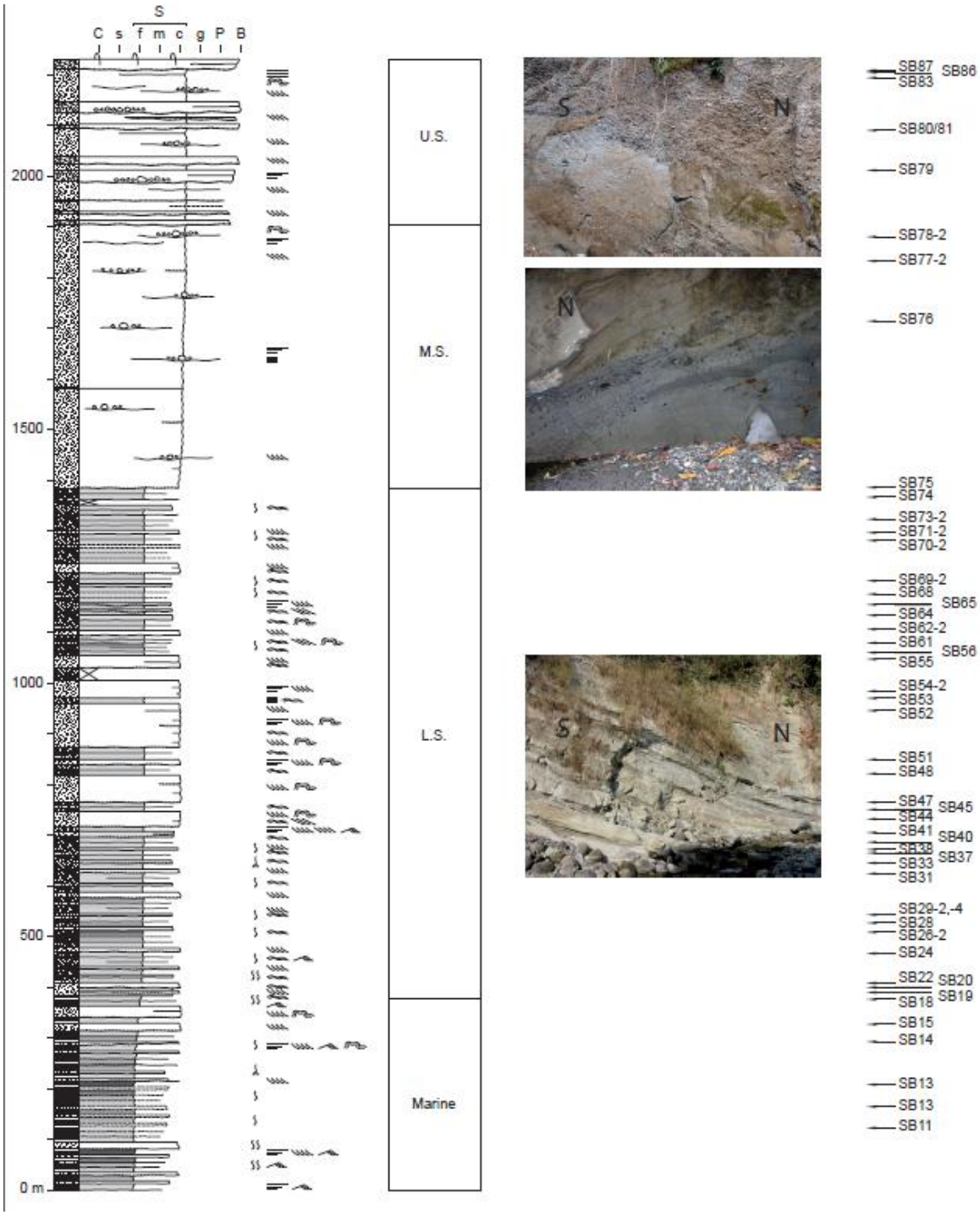

Figure 2.6: Stratigraphic column of the Samdrup Jongkhar transect measured and drawn by Laurie Barrier. Beside the column are the transitions between subgroups of the Siwalik, transect photos and sample locations. L.S.: Lower Siwalik; M.S.: Middle Siwalik; U.S.: Upper Siwalik. Preliminary facies analysis by Laurie Barrier has shown the beginning of the transect to be made up of marine sediments.

CHAPTER III: METHODOLOGY

3.1 O AND H STABLE ISOTOPES AND THEIR APPLICATION TO PALEOCLIMATE STUDIES

Past climates can leave their imprints in both continental and marine geologic records. For paleoclimate reconstructions stable isotopes of H, O, and C are the most commonly used geochemical proxies, since the isotopic ratio is sensitive to the environmental conditions. Methods have been developed to determine the paleotemperature, amount of precipitation and paleoelevation of local settings (Hoefs, 2009). Marine records hold a global isotopic ratio due to the well mixed nature of the global system, whereas the continental records are affected by regional factors. Continental paleoclimate records are preserved naturally within the isotopic compositions found in tree rings, organic matter, carbonates and hydroxyl-bearing minerals, such as clay minerals (Hoefs, 2009).

The application of isotope studies with clay minerals depends on the knowledge of isotope fractionation factors between clay minerals and water, the temperature and the final exchange time frame (Hoefs, 2009).

3.1.1 BACKGROUND TO ISOTOPES AND FRACTIONATION

Isotopes of an element have the same number of protons but different amounts of neutrons within the atomic nucleus. Therefore isotopes of a certain element have the same atomic number but different atomic masses, and ionic radii, which is the main cause for isotopic fractionation in nature. Fractionation is the process by which isotopes are preferentially included or excluded from a system resulting in isotopic ratios within a particular phase or region to differ from one another, for example $^{18}O/^{16}O$ ratio is different in rainwater than ocean water (Drever, 1997). Absolute isotopic values are not convenient for use in analysis, instead δ notation is used where the δ values are represented in parts per thousand (‰) between the ratio in the sample and the ratio in the element standard, as shown in Equation 1 (Rumble & Hoering, 1994) for oxygen isotopes.

$$\delta^{18}O = \frac{\left[\left(^{18}O/^{16}O\right)_{sample} - \left(^{18}O/^{16}O\right)_{standard}\right] \times 1000\ ‰}{\left(^{18}O/^{16}O\right)_{standard}} \quad \textbf{(1)}$$

Natural isotopic fractionation in water occurs through several processes. The physical processes of greatest importance to meteorology, hydrology, and glaciology are condensation and evaporation (Dansgaard, 1964; Drever, 1997). Physical fractionation processes involve vapour and liquid fractionation during evaporation and condensation. When liquid water and water vapour are in equilibrium the vapour is isotopically lighter than the liquid phase (which is isotopically heavier). If one phase is isotopically heavier than another, it is enriched in the heavier isotope, such as Deuterium (D) or ^{18}O and depleted in the lighter isotope, ^{1}H or ^{16}O respectively. When water vapour condenses to form rain, fractionation takes place in which the liquid is isotopically heavier than the vapour, so that the heavier isotopes are "rained out." As the rain continues to fall the vapour will become progressively depleted in heavy isotopes and therefore the rain will become subsequently lighter through the process of Rayleigh fractionation (Drever, 1997). Consequently, the further the distance an airmass travels, the lighter the isotopic values will be. As well, during large storm events with greater amounts of precipitation, the rain will become enriched in lighter isotopes (Stern et al., 1997). In general the hydrogen and oxygen isotopes in precipitation become progressively lighter from the equator to the poles, from the coast inland, and from lower to higher elevations (Drever, 1997). Isotopic values of precipitation are therefore controlled by the atmospheric patterns (Stern et al., 1997). The isotopic composition of recent meteoric water plots close to the global meteoric water line (GMWL) for a given region, the regional local water line deviates by an amount relative to the fractionation factor between hydrogen and oxygen (Fig. 3.1) (Hoefs, 2009).

Isotopic compositions of precipitation vary depending upon regional location, from season to season and even from one rainstorm to another. These deviations are due to different air mass circulations (i.e. moisture sources), different atmospheric temperatures, and different amounts of evaporation as the raindrop falls through the air (Drever, 1997).

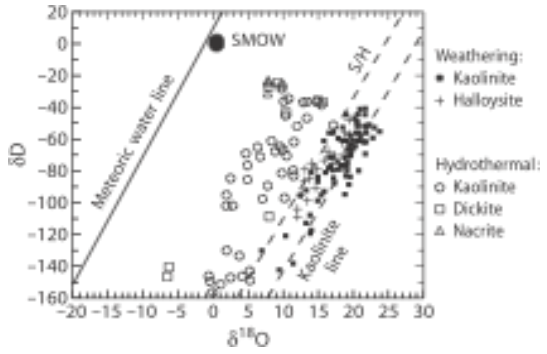

Figure 3.1: Meteoric water line, kaolinite weathering and the supergene/hypogene (S/H) lines are given for reference (From Sheppard et al., 1996; Hoefs, 2009). δD and $\delta^{18}O$ values for kaolinites and related minerals from weathering and hydrothermal environments.

3.2 ANALYTICAL PROCEDURES

3.2.1 CLAY MINERAL SEPERATION

Particular care should be taken during the separation of the clay minerals from a sample. No grinding motion should be used for clay mineral separation; otherwise the coarser minerals could be ground down to the clay fraction grain size. Thus the sample cannot be pulverized using a disk mill. For the analyses of clay minerals, each paleosol sample was first crushed with a rock hammer, and then a fraction of each sample was soaked in deionized water overnight. A mortar and pestle was used to further crush the soaked material. The final step for disaggregating the material was to use a laboratory blender (Waring®) to suspend the clay minerals followed by treatment in an ultrasonic bath to separate any fine grained aggregates.

Prepared material was treated with glacial acetic acid (<0.3 molar) to remove carbonates from the paleosol. Stronger acids, such as hydrochloric acid, could damage the crystal structure of the clay minerals which could cause inaccurate X-ray diffraction (XRD) results (Moore & Reynolds, 1997). Once the samples stopped effervescing they were rinsed free of the acid with deionized water by centrifugation, five to six times, until sediments remained suspended in the water. The separation of <2 μm size fraction was performed with a centrifuge, where the time was calculated using equation 2 (Moore et al., 1997):

$$T = \frac{9\eta \ln \frac{R_2}{R_1}}{8\pi^2 N^2 r^2 (\rho + \rho_0)} + \frac{2(t_a + t_d)}{3} \quad \textbf{(2)}$$

The parameters for Equation 2 are outlined in Table 3.1 and the centrifuge values for this project are displayed in Table 3.2 at two values of room temperature, which was the temperature range in the laboratory during sample preparation. The material left in suspension, after 100 s of centrifugation at 800 rpm, was the <2 μm size fraction. This fraction was suctioned out of the vial and dried in an oven at <60 ˚C. Aliquots of 30 mg were prepared for oxygen and hydrogen mass spectrometry and smear slides for XRD. After centrifugation some of the samples left two separations within the vial. In these cases each of the layers was sampled and reseparated, resulting in varying grain sizes of <2 μm, 2-5 μm, and <5 μm. In such samples all three grain size fractions were analyzed to see if isotopic alteration occurred. See Appendix A for clay separation details.

Table 3.1: Parameters for Equation 2.

T= total time (s)	R_2= final distance from rotation axis (cm)
t_a= time of acceleration (s)	r= particle radius (cm)
t_d= time of deceleration (s)	*N*= angular velocity (rev/s)
η= viscosity (poises)	ρ= density of the particle (g/cm^3)
R_1= initial distance from rotation axis (cm)	ρ_0= density of water (g/cm^3)

Table 3.2: Centrifugation values for the samples and centrifuge.

T (˚C)	η (poise)	R_1 (cm)	R_2 (cm)	*N* (rev/s)	r (cm)	ρ (g/cm^3)	ρ_0 (g/cm^3)	t_a (s)	t_d (s)	π	T (s)
20	0.01005	6.8	9.2	13.3	0.0002	2.65	1	24	50	3.14	79
25	0.0091	6.8	9.2	13.3	0.0002	2.65	1	24	50	3.14	76

3.2.2 OXYGEN MASS SPECTROMETRY

The oxygen isotopic composition of each sample was measured by Finnigan MAT 253 isotope ratio mass spectrometer in the Stable Isotope Lab at the University of Lausanne, Switzerland. To prepare the powdered sample for analysis, 0.5 to 2mg was mixed with 1 to 4 mg of BaF, to decrease the amount of sample splatter during the analysis, and loaded onto a small Pt-sample holder. Pure fluorine is preferred to BrF_2 since it reacts with most minerals (Rumble & Hoering, 1994). The sample holder was placed within the analysis chamber,

which was vacuumed to 10^{-6} mbar and pre-fluorinated overnight. While the samples were immersed in 50 mbar of pure fluorine a CO_2-laser beam, shot at the sample holder, and heated the individual sample within the analysis chamber. As the clay minerals were heated they quickly reacted with the F releasing O_2, while the surrounding unheated material remained unreacted (Rumble & Hoering, 1994). Excess fluorine was separated from the O_2 through a reaction with KCl at 150˚C, where the extracted O_2 was collected in a molecular sieve (mesh size 5 Å) immersed in liquid nitrogen. As the O_2 was reheated it expanded into the inlet for the mass spectrometer.

Oxygen isotope compositions are given in standard δ-notation, expressing the sample composition relative to the standard reference gas of VSMOW (Vienna Standard Mean Ocean Water) in permille (‰). The composition was determined using Equation 1 (Rumble & Hoering, 1994), where the isotopic ratio of the standard (VSMOW) $(^{18}O/^{16}O)_{standard}$ is equal to 2,005.20±0.43 (Baertschi, 1976).

The average precision of the commonly used replicate standard of the in-house quartz, NBS-28 quartz, is ± 0.1‰ with the standard value at +9.6 ‰, (T. Vennemann pers. com., Aug., 2011) and the accuracy for $\delta^{18}O$ values are better than ± 0.2 ‰.

3.2.3 HYDROGEN MASS SPECTROMETRY

Sample preparation for hydrogen mass spectrometry involved removing all moisture from the surrounding air, so that the H in the present atmosphere would not affect the analysis. 1500 to 2500 μg of sample was weighed into silver capsules for solids (3.3 x 5 mm) and folded shut into a cube shape. These silver capsules were heated to 200˚C in a vacuum chamber for 4-5 hours in order to extract the moisture. Each sample was individually isolated from the surrounding air by melting the beryl glass carrier vial (attached to the vacuum) which was cut off and sealed with a blow torch with the sample capsule inside.

The hydrogen isotope analysis technique was performed with a ThermoFinnigan MAT DELTAplus XL isotope ratio mass spectrometer at the University of Lausanne. The procedure involves the reduction of solid hydrous

clay samples through reaction with glassy carbon at high temperatures (Sharp et al. 2001). Each sample was dropped individually into the furnace (Fig. 3.2), after breaking the carrier vials. At 1450˚C hydrogen is liberated by the reaction of clay with carbon in a helium carrier gas. These gases were then separated in a gas chromatograph and analyzed in the mass spectrometer. Two standards were run after every ten samples in order to calibrate the results. The two standards used were in house kaolinite 17, and a G1 biotite, which have different concentrations of water within their mineral structure.

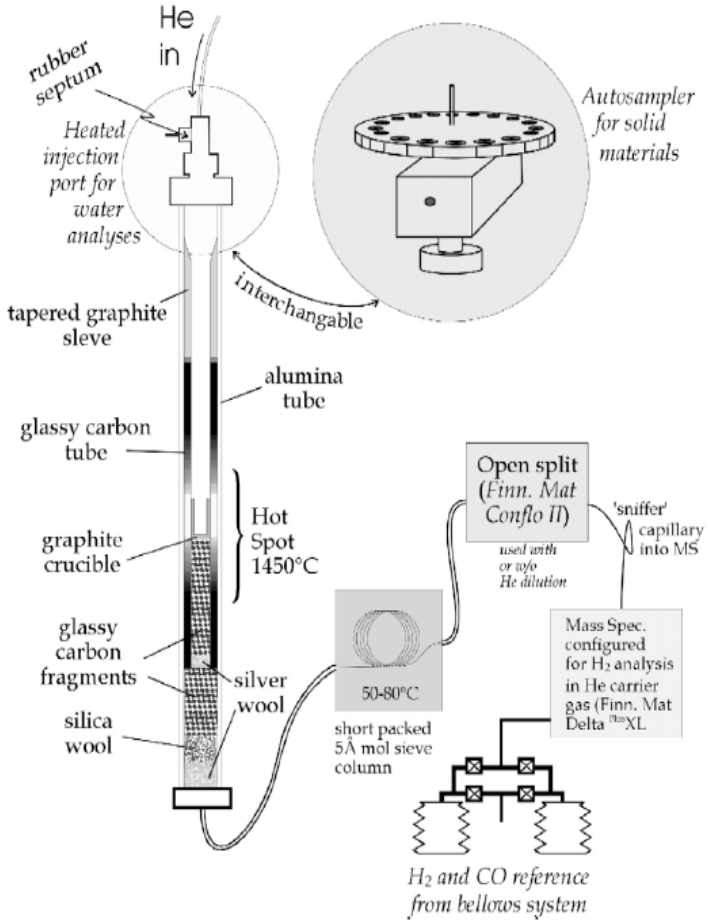

Figure 3.2: Schematic diagram of the extraction system used to reduce and heat the clay samples to extract hydrogen gas. The sample falls into the graphite crucible, within the furnace set at 1450˚C. There the sample is reduced to H_2 which is passed through a molecular sieve column, into the open split and then into the mass spectrometer. Within the mass spectrometer reference gases for hydrogen are introduced for comparison. From Sharp et al. (2001).

The results are given in standard δ-notation, expressed relative to VSMOW reference gas in permille (‰) with Equation 3.

$$\delta D = \frac{\left[\left({}^{2}H/{}^{1}H\right)_{sample} - \left({}^{2}H/{}^{1}H\right)_{standard}\right] \times 1000\ ‰}{\left({}^{2}H/{}^{1}H\right)_{standard}} \quad \textbf{(3)}$$

(Rumble & Hoering, 1994).

where the isotopic ratio of the standard (VSMOW) is $({}^{2}H/{}^{1}H)_{standard}$ equal to 155.76±0.1 ppm (Hagemann et al., 1970). The precision for in-house kaolinite and G1 biotite standards was better than ± 2‰ for this method (T. Vennemann, pers. com., Aug., 2011), and all results were normalized using a value of -125‰ for the kaolinite standard and -65‰ for the G1 biotite.

3.2.4 X-RAY DIFFRACTION

Clay mineral assemblages can be composed of a mixture of detrital and authigenic components. Although this study does not prove the presence of authigenic as opposed to detrital clay components the identification of the mineralogy of the sample was required to interpret the isotopic compositional variation (Hoefs, 2009). Clay minerals are most commonly identified using X-Ray Diffraction (XRD) patterns of oriented aggregates that enhance the basal reflections (Moore & Reynolds, 1997).

The premise behind XRD is that the x-rays reflected are similar to the spacing of atoms in the crystal structure of most minerals (1 or 2 Å) (Nesse, 2000). The angle of incidence where the diffraction maxima will occur can be calculated for a certain wavelength of x-rays and interplanar (d) spacing between atoms in a crystal structure (Nesse, 2000). The relationship is known as Bragg's Law, shown in Equation 4 and explained in Figure 3.3.

Samples for XRD measurements were prepared using the smear method (Moore & Reynolds, 1997). To prepare the samples for XRD they were first finely crushed into a powder and placed on the frosted side of a petrographic slide. Droplets of water were added to spread the minerals out and with another slide placed on top the clay was then smeared across the slide. Since the clay minerals were randomly oriented within a saturated powder upon the slide, resulting in a random orientation of interplanar (d) spacings, the slide and detector were

rotated to record the wide range of reflected orientations. The slide pivots relative to the X-ray beam to allow the angle of incidence to vary from 0 to 90°. The detector moves at twice the angular speed between the sample slide and X-ray tube to create the 2θ angle required to record the deflections (Fig. 3.4; Nesse, 2000).

$$n\lambda = 2d \sin\theta \quad \textbf{(4)}$$

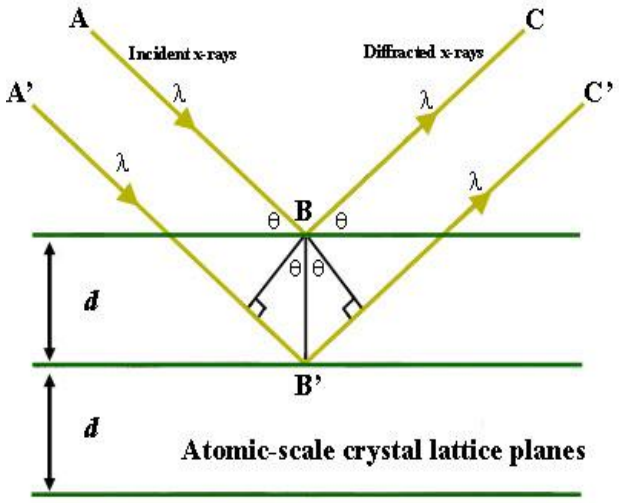

Figure 3.3: Diffraction diagram illustrating Bragg's Law. The incident X-rays diffract from the parallel atom planes. Constructive interference of the diffracted rays will provide a peak in intensity when the distance between path ABC and A'B'C' differentiates by an integer (*n*) number of wavelengths (λ). From Carlton College (2011).

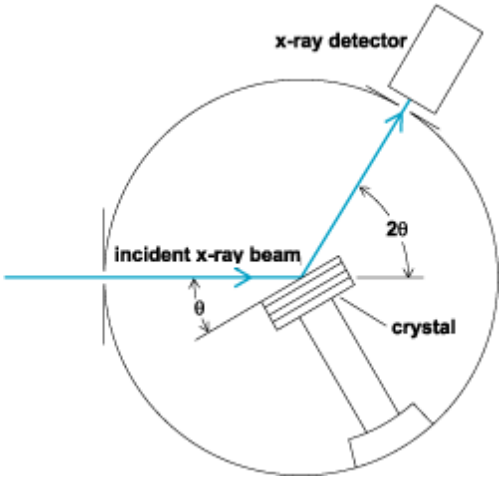

Figure 3.4: Schematic diagram of the movement of the sample slide with respect to the detector by 2θ. From Columbia University (2011).

Detected x-ray peak intensity relative to the 2θ angle of the detector was measured using "X'Pert Quantify" software. The mineral's chemical components were then run through the database created by the International Centre for Diffraction Data with the software "X'Pert HighScore." This software ran the pattern of peak intensities from each sample against the compiled data of a wide range of chemical species in the system. A list was created by the software with probabilities of chemical species that match closely to the chemical species measured within the slide. Geological background and previous literature, as well as the highest probabilities determined by the software were all used to determine the final analysis of the minerals within each sample slide (Appendix B).

Difficulties in the methods of clay mineral analysis by XRD arise due to their fine grain size with similar principal characteristics. Basal spacing is used to decipher between different groups of clay minerals. To distinguish between clay minerals of similar basal spacing, other techniques can be used. For many clay minerals the procedures include a comparison of air-dried and ethylene glycol-solvated prepared samples (Moore, et al., 1997). The shifts in strong reflections have been determined and can therefore be used for sample analysis. While this is the case for the clay mineral smectite, other minerals require a few more processes evolving from this procedure.

In order to distinguish illite from glauconite the samples are heated to 550˚C with no interference of ethylene glycol solvation. From this analysis the glauconite would have lower intensity peaks than illite with a very weak, to non-existent 002 reflection due to a heavy scattering from the octahedral iron (Moore et al., 1997).

Chlorite and kaolinite have different structures and occur in different geological regions but can be difficult to differentiate in mutual mixtures, and most difficult when high-Fe chlorites are involved. In this situation the sample may be treated chemically or heated and then reanalyzed. The aggregate technique is used to determine the chlorite group from the kaolinite group. It involves heating the samples to 500˚C, at which point kaolinite become amorphous to x-rays and its diffractions disappear due to break down of the

lattice (Nagelschmidt, 1946; Moore et al., 1997). Heating of the chlorite minerals causes dehydroxylation of the hydroxide sheet with detailed changes to the diffraction pattern. The opposing technique is used to determine the presence of kaolinite, in which the sample should be boiled for two hours in hydrochloric acid (HCl), dissolving the chlorite minerals. These techniques will suggest if chlorite or kaolinite is present or absent, however it will not give the complete results if the sample contains both (Moore et al., 1997).

Vermiculite displays little change in diffraction patterns from air-dried to glycol solvation and when mixed with chlorite can have problems in identification. This difficulty is resolved by K-saturation of the sample or heating the sample to 300˚C for an hour. These treatments cause the vermiculite to collapse, changing its diffraction pattern to one similar to biotite and glauconite (Moore et al., 1997).

Due to the time constraints and the scope of this thesis, these further procedures for the identification of clay minerals by XRD were not included and are therefore considerations for further research.

CHAPTER IV: RESULTS

4.1 X-RAY DIFFRACTION: CLAY PROVENANCE

The XRD analyses indicate that the samples are made up predominantly of clay group minerals and fine-grained quartz. The difficulty with analysing clay minerals arises due to their small grain size. Once the software ran the analysis and the highest probabilities determined were listed, my geological background and knowledge of previous literature was the basis for the final analysis of the minerals within each sample slide. The result is a match of 2-3 minerals with the most similar highest probability peak intensities to the major analysis peaks, as detecting more minerals would be difficult. The acquired XRD patterns for each sample are displayed in Appendix B, while the representative XRD patterns are shown in Figure 4.1. Within the samples from the section, kaolinite and illite are dominant, smectite is observed throughout the transect within a moderate number of samples, and chlorite is observed within the Lower Siwalik samples and in decreasing amounts of samples up the section (Fig. 4.2). These results suggest that the samples consist dominantly of clays minerals rather than detrital micas, which would have obscured the isotopic values obtained. Detrital hydrous phyllosilicates, such as muscovite, would yield isotopic values of metamorphic fluids instead of the meteoric water. The mineralogy of the samples, determined by XRD analysis, are clay minerals that would have formed by the weathering and erosion of the Himalayan basement rocks (Stern et al., 1997), and presumably deposited in equilibrium with meteoric waters. Clay minerals in the Siwalik Group are considered to be authigenic (i.e., pedogenic) (Stern et al., 1997), and therefore the isotopic analyses of the minerals yield the compositions of meteoric water instead of metamorphic fluids from micas. Previous studies have shown the Siwalik clay minerals from the Potwar Plateau, Pakistan to have a covariation of smectite $\delta^{18}O$ values and calcite $\delta^{18}O$ values through time, which suggests a pedogenic origin of smectite. Kaolinite $\delta^{18}O$ values were shown to vary similarly with the smectite $\delta^{18}O$, which is expected for pedogenic kaolinite (Stern et al., 1997).

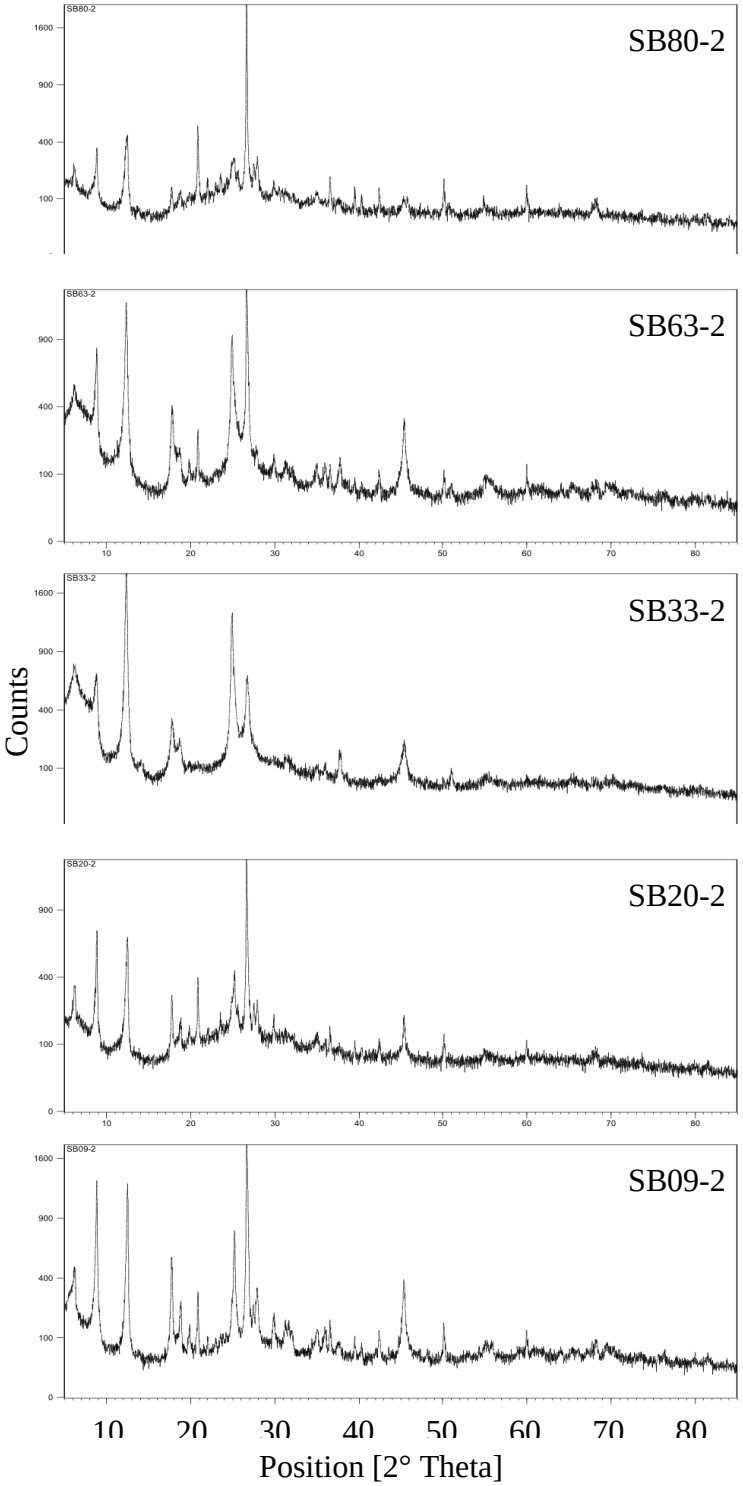

Figure 4.1: Stacked XRD results from representative samples throughout the transect. These are the resulting graphs from the XRD analysis of 5 samples stacked upon each other for an average overall view of the XRD data showing the similarities and differences between sample analyses. The x-axis is measured as the position of 2° theta diffraction, and the y-axis is measured as the counts or intensity of the diffracted x-rays.

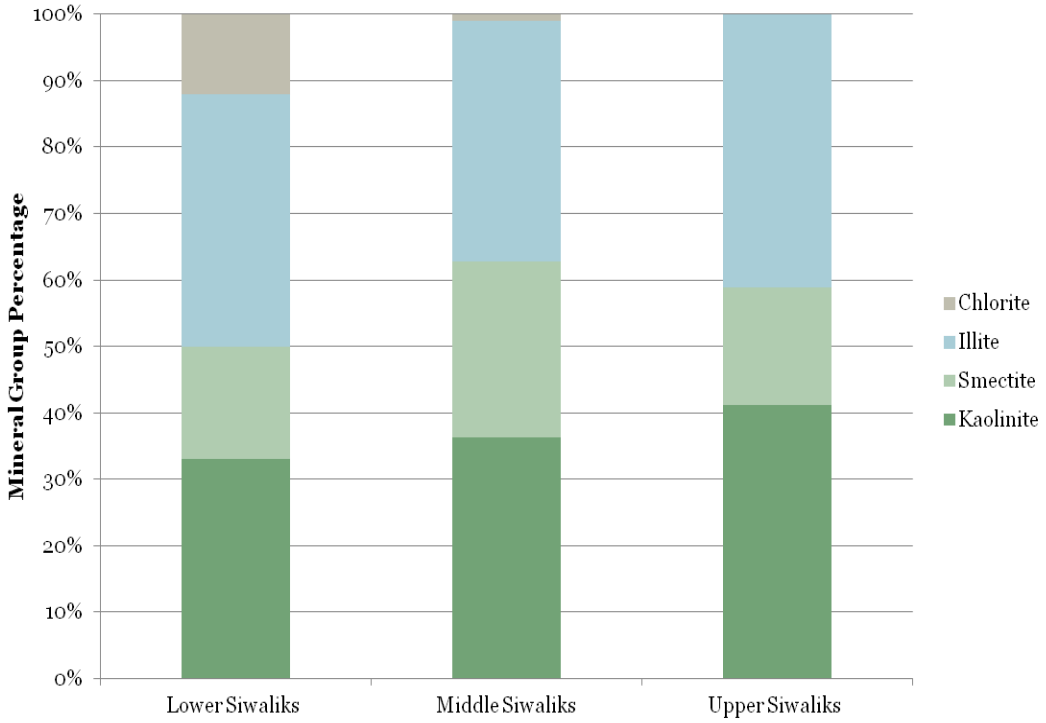

Figure 4.2: Clay mineralogy graph, displaying the clay minerals represented as the percentage of samples in which the minerals were observed. For this graph, from each sample XRD analysis the clay minerals were recorded. For each subgroup the clay minerals found within each of the samples were recorded. All the observed clay minerals within the samples for each subgroup were calculated as a percentage of the total clay minerals found within the subgroup.

4.2 OXYGEN AND HYDROGEN COMPOSITION

The isotope data for both δD and $\delta^{18}O$ are shown in Figure 4.3 alongside the stratigraphic column from the Samdrup Jongkhar transect. δD and $\delta^{18}O$ of the clay minerals are plotted as per mille (‰) values compared to the reference gas VSMOW. Throughout the analysis, multiples of several samples were measured and the average value of these multiples was used within Figure 4.3 as the final values (Appendix C). The gaps in isotopic data points within the Upper Siwalik section are due to a lack of paleosol horizons in the unit. The $\delta^{18}O$ values range from 11.7 to 14.3‰ with a mean value of 12.2‰ ± 0.2‰. δD values range from -81.5 to -103.8‰ with a mean value of -86.8‰ and precision better than ±2‰. Excess deuterium (D-excess) is calculated from the δD and $\delta^{18}O$ values of the clay minerals as in Equation 5. D-excess traces the moisture source of the monsoon rain based on the correlation between the d-excess

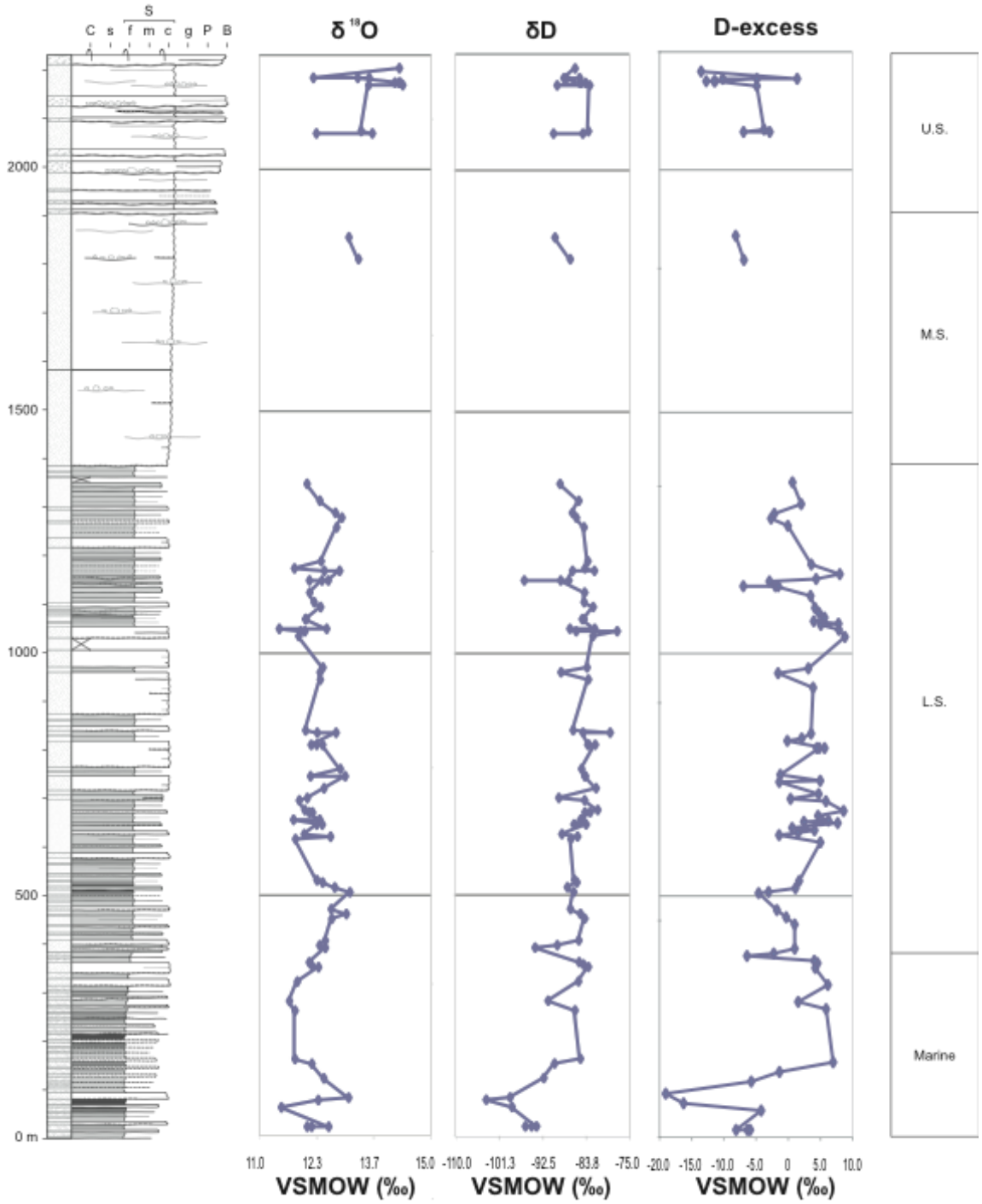

Figure 4.3: δD and $\delta^{18}O$ isotopic composition of the clay minerals alongside the stratigraphic thickness. δD and $\delta^{18}O$ are recorded in per mille (‰) as compared to the standard VSMOW. D-excess is the calculated isotopic value from equation 5 in VSMOW recorded in per mille (‰). The stratigraphic column was measured and drawn by Dr. I. Coutand and Laurie Barrier with the sample site locations from the Samdrup Jongkhar transect. The observed transitions between Siwalik subgroups are displayed to the right; marine facies, L.S.: Lower Siwalik, M.S.: Middle Siwalik, U.S.: Upper Siwalik.

and the relative humidity over the ocean, as the potential source of the water vapour (Pang et al., 2004).

$$\text{D-excess} = \delta D - 8\,\delta^{18}O \quad \textbf{(5)}$$

(Dansgaard, 1964). Both isotopic values show a cyclic pattern of variability throughout the Lower and Middle Siwalik, whereas there is no continuous isotopic record of the Upper Siwalik to observe a pattern within the data. Three first-order cycles are observed, the first begins as a peak in $\delta^{18}O$ of 13.1‰ at 100 m and decreases towards a minimum of 11.7‰ at 300 m where it then increases to 13.1‰ again at 500 m. A similar cycle is observed through 500 m to 740 m and again from 740 m to 1280 m. The second and third cycles are not as smooth as the first, they have many second or third order cycles within the first, but they retain similar values for the maximum and minimum values (±0.3‰). These cycles are also observed within the excess deuterium record. With the known stratigraphic ages, the frequency of the first and second order variations could be compared to the calculated summer insolation variations (Laskar et al., 2003) and to the well-established paleoclimate record (Zachos et al., 2001), which occur on the time scale of ~65-0 Ma.

CHAPTER V: DISCUSSION

5.1 PALEOSOLS

The use of hydroxyl-bearing minerals for paleoclimate reconstructions raise a concern for whether or not the clay minerals are detrital, authigenic or possibly a mixture of both (Hoefs, 2009). Some clay minerals, for example illite, can be formed by weathering, diagenesis or metamorphism, therefore it is important to identify the formation of these minerals to correctly apply the results of an isotopic analysis. If these clays came in contact with metamorphic fluids and were affected by diagenesis and low grade metamorphism the isotopic values could not be used as paleoclimate indicators. The XRD analysis for this study demonstrated that the samples are in fact predominantly clay minerals with some fine grained quartz. The quartz fraction within the samples implies some detrital fraction; however quartz is not hydroxyl bearing. Other forms of detrital materials have been found within the Siwalik Group. The <2 μm fraction extracted from the Siwalik Group sediments is made up of clay groups; illite, chlorite, kaolinite, and smectite with some mixed-layers clays (Huyghe et al., 2005). Through illite-crystallinity methods, detrital illite has been found within the Siwalik Group along with authogenic smectite-illite minerals (Huyghe et al., 2005). Sericite (a fine-grained series of muscovite) has been observed within the units of the Lesser Himalayan Sequence, and could also have deposited as detrital fraction within the paleosol units (McQuarrie et al., 2008).

The Siwalik clay minerals at the Potwar Plateau, in northern Pakistan are of pedogenic or authigenic origin due to four main observations (Stern et al., 1997). (a) within the Siwalik paleosols the proportion of smectite and kaolinite is higher than in nearby sequences of unweathered mudstone; (b) the $\delta^{18}O$ values in the smectite and kaolinite are consistent with being in equilibrium with soil water at surficial temperatures; (c) sediment cores from the Bengal Fan provide chemical and isotopic compositions of smectite and kaolinite-rich clay fractions formed by the weathering of the Himalayan foreland rocks on the Indo-Gangetic Plains; (d) the variations in $\delta^{18}O$ values of smectite were synchronous to the $\delta^{18}O$ values of the pedogenic calcite within the stratigraphy and therefore can be used

to an equal extent as the calcite. These observations were the principal basis for interpreting the clays from the Siwalik Group as authigenic to be used as climate proxies within this study.

5.2 PALEO-METEORIC WATER

To interpret the isotopic composition of clays in the sense of paleoclimate records, one has to calculate the isotopic composition of the waters involved in the transformation of the rocks to clay. This requires the knowledge of the paleo-temperature of the water and the fractionation factor of isotopes between water and clay. Because of many unknowns I have taken several approaches and selected the mutually consistent results. In a δD vs. $\delta^{18}O$ diagram the clay isotopic compositions cluster closely (Fig. 5.1, the right hand side); and two outliers of low δD and high $\delta^{18}O$ correspond to the samples at the bottom and the top of the

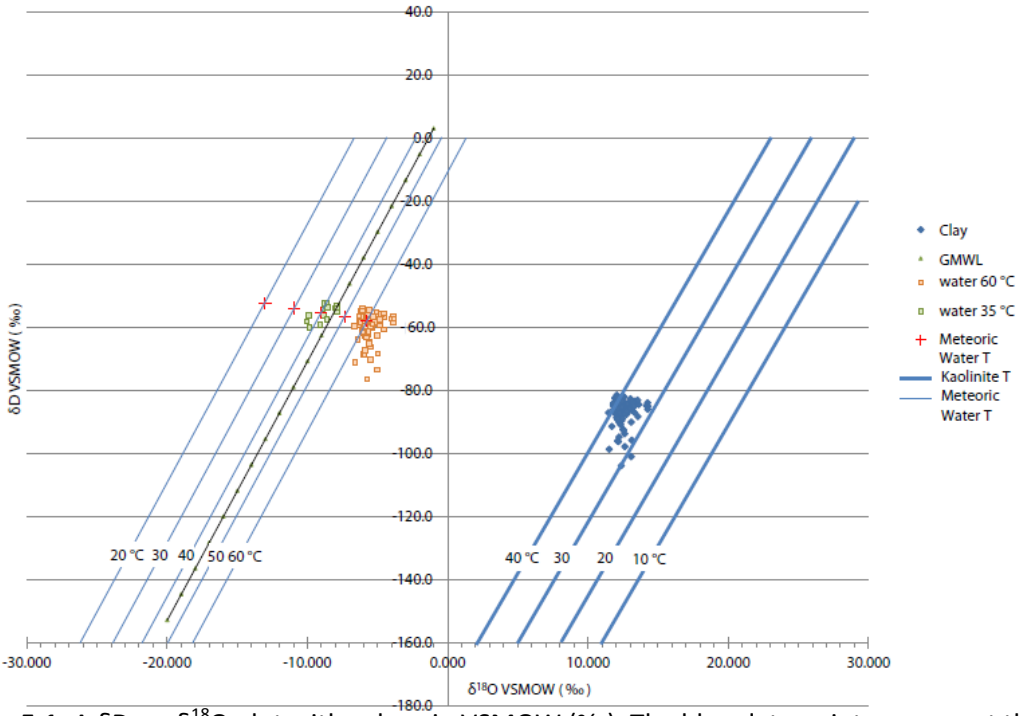

Figure 5.1: A δD vs. $\delta^{18}O$ plot with values in VSMOW (‰). The blue data points represent the clay sample isotopic compositions from the stable isotope analysis, as shown in Table 4.2. The kaolinite line for temperatures of 10-40 °C (from Sheppard, et al., 1996) overlay the data points. Meteoric water isotopic values were calculated from the clay sample isotopic compositions using Equations 6.0 and 7.0 and plotted in orange for 60 °C and in green for 35 °C. The mean isotopic composition of the meteoric water in equilibrium with the clay samples for calculated temperatures ranging from 20-60 °C are plotted as red crosses. The Global Meteoric Water Line (GMWL) is also plotted as green triangles with a black trend line for reference.

stratigraphic column. When these outliers are disregarded the mean isotopic composition of clay is -12.03 ± 0.46‰ $\delta^{18}O$ and -85.59 ± 2.57‰ δD.

The empirically-derived water lines for kaolinite at 10-40 °C (Sheppard et al., 1996) in the same plot indicate the temperature of water with which clays equilibrated. The data suggests the average temperature of kaolinite in equilibrium with meteoric water to be 40 °C, since the cluster of clay isotopic values are closest to the 40 °C kaolinite line, with outliers ranging from 30 – 35 °C. A more quantitative paleo-temperature calculation has been developed only for smectite (Delgado et al., 1996):

$$3.54x10^{6}T^{-2} = \delta^{18}O_{sm} - 0.125\delta D_{sm} + 8.95 \quad \textbf{(6)}$$

Assuming all the clays in the investigated samples were smectite, taking the mean isotopic value yields paleo-temperatures of ~59.6 °C.

Meteoric water in equilibrium with the clay minerals contains a different isotopic composition than that of the clay minerals due to fractionation processes, which are different for different isotopes and for each mineral. The meteoric water isotopic compositions can be calculated from the clay isotopic compositions using the hydrogen clay-water fractionation equation (Sheppard et al., 1996):

$$1000\ln\alpha_{K-W} = -2.2\times10^{6}\times T^{-2} - 7.7 \quad \textbf{(7)}$$

and the oxygen kaolinite-water fractionation equation(Sheppard et al., 1996):

$$1000\ln\alpha_{K-W} = 2.76\times10^{6}\times T^{-2} - 6.75 \quad \textbf{(8)}$$

where T is temperature in K. The mean meteoric water compositions are represented in Figure 5.1 as red crosses for temperatures of 20-60 °C from left to right (values shown in Appendix C: Table C3). The question is, for which temperature should the calculations be used? The kaolinite line suggests 40 °C; the smectite paleo-temperature calculation ~ 50 °C; the preliminary vitrinite reflectance data have shown that the maximum burial temperature of the Siwalik sediments was 60 ± 10 °C (Fig. 5.2); and the modern average annual temperature of the Himalayan foreland is 25 °C (Ohsawa, 1991) and is believed to have remained constant since the deposition of the Siwalik sediments even with the

northward drift of India during the period (Quade et al., 2011). From this evidence, the Siwalik sediments would have equilibrated in meteoric waters within a temperature range from the average temperature of the foreland basin, to the maximum temperature from depth of burial, from 25-60 °C.

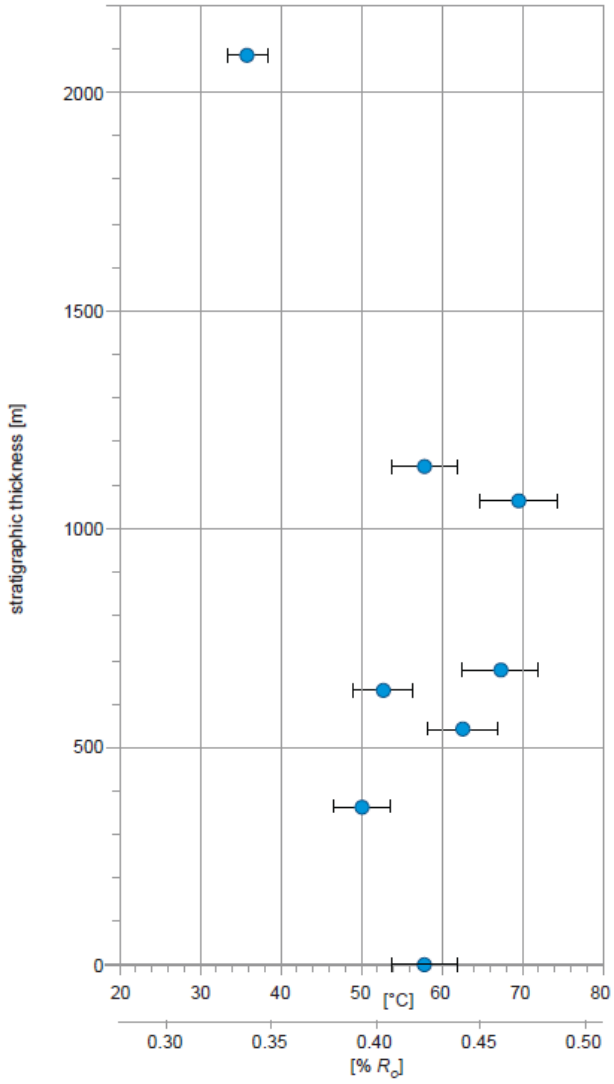

Figure 5.2: Temperature vs. stratigraphic thickness graph of the vitrinite reflectance data, sampled and measured by D. Grujic. Temperature is calculated from the R_o data (the vitrinite reflectance data). Note that the mean value is 60 ˚C ±10 ˚C, describing the maximum temperature attained from burial. This temperature would correspond to ~2-3 km depth considering the geothermal gradient as 20-30 ˚C/km (Biswas et al., 2007).

5.3 LOCAL METEORIC WATER LINE

Hydrogen isotopes are fractionated in proportion to oxygen isotopes due to corresponding differences in vapour pressure in all processes involving evaporation and condensation, the global meteoric water line (GMWL) is generally the correlation between hydrogen and oxygen distributions within the meteoric waters as shown by Equation 9 (Hoefs, 2009).

$$\delta D = 8\,\delta^{18}O + 10 \quad \textbf{(9)}$$

The local meteoric water line (LMWL) is different than the GMWL due to the local region's fractionation factor; all the isotopic compositions of meteoric water for the region should plot upon this line on a δD vs. $\delta^{18}O$ plot (Hoefs, 2009). Isotopic compositions of meteoric water samples across eastern Bhutan (collected in 2007, 2008 and 2011) are plotted upon a δD vs. $\delta^{18}O$ plot, which result in the eastern Bhutan meteoric water line (Fig. 5.3). The calculated meteoric water isotopic compositions from the samples were compared to the eastern Bhutan LMWL.

Because the water isotopic composition is highly elevation dependent (Quade et al., 2011) and since all the meteoric water samples were collected at higher elevations than the foreland sedimentary basin, the present isotopic composition of water at an elevation of 100 m was estimated based on elevation vs. isotopic composition graphs (Fig. 5.4 a & b). The Siwalik sediments were deposited at an elevation of 100 m and after uplift and deformation of the Subhimalaya they remain, at present, at an elevation of 100 m, where the meteoric water isotopic composition is approximately -4.2 ±1‰ $\delta^{18}O$, -34±10‰ δD. In the case that water in equilibrium with meteoric water should plot upon the LMWL, the best approximation for the meteoric water isotopic composition in equilibrium with the clay minerals is at 50° C (Fig. 5.3). This is estimated because the mean isotopic composition of the meteoric water for 50 °C (shown by a red cross on the 50 °C water line) falls upon the eastern Bhutan meteoric water line. This results in the mean isotopic composition of meteoric water in equilibrium with the Siwalik samples to be approximately -7.4‰ $\delta^{18}O$, -56.8‰ δD. This results in an increase in $\delta^{18}O$ by ~3.2‰ since the deposition of the

Siwalik. The temperature of 50 °C could be reached by a burial depth of 1.5-2 km, when considering the geothermal gradient in the foreland basins of the region at 20-30 °C/ km (Rao et al., 1976; Zahid et al., 2005; Biswas et al., 2007). This is a realistic value considering the preserved thickness of the Siwalik sediments in the eastern Bhutan and is also consistent with the geothermal gradients inferred for the time during the Siwalik deposition (Bernet et al., 2006). When this value from the deposition of the Siwalik sediments is compared with the value of present eastern Bhutan meteoric waters at the same elevation (100 m) the paleo-water values are significantly lower in both δD and $\delta^{18}O$ than at present.

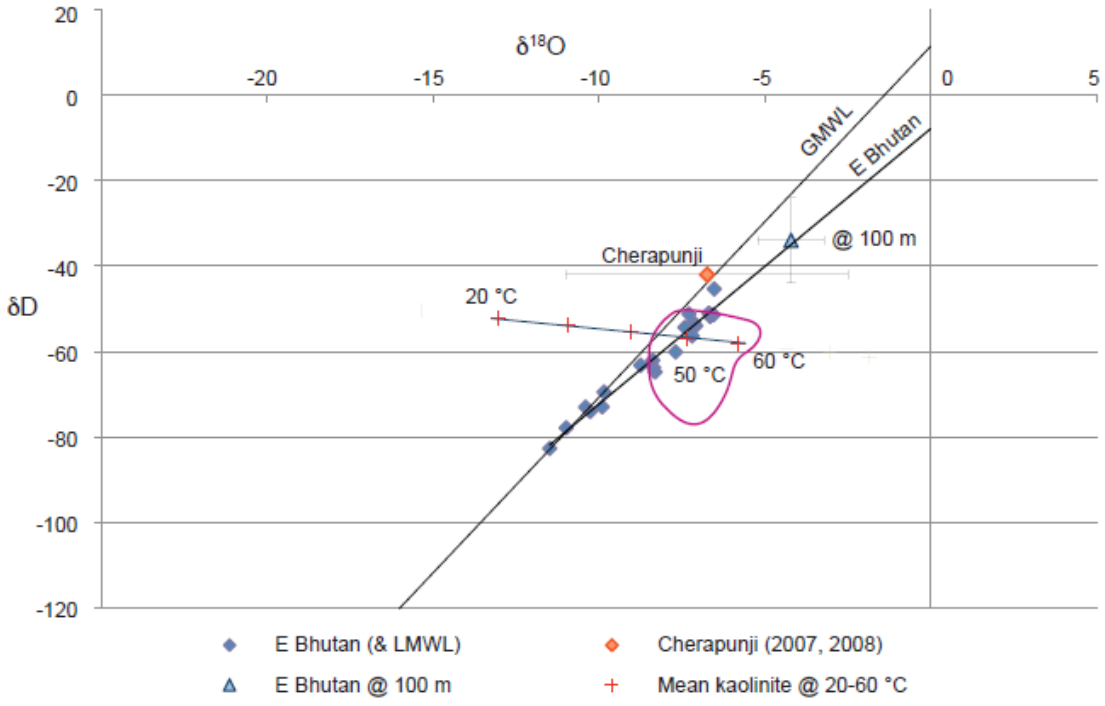

Figure 5.3: A close up of the meteoric water isotopic compositions from Figure 5.2 within a δD vs $\delta^{18}O$ plot with values in VSMOW (‰). The red crosses represent the mean isotopic composition of meteoric water in equilibrium with the clay samples calculated for temperatures of 20-60 °C. Samples of meteoric water across eastern Bhutan (taken since 2007) are plotted with a trend line resulting in the eastern Bhutan local meteoric water line (LMWL). The isotopic composition at 100m elevation within the E Bhutan meteoric water line has a mean value of -4.2‰ $\delta^{18}O$, -34‰ δD. The pink outlines the meteoric water isotopic data distribution of the samples at 50 °C, with a mean value of -7.4‰ $\delta^{18}O$, -56.8‰ δD. The GMWL overlays the figure, the isotopic composition recorded from 2007-2008 at Cherapunji is plotted, and falls upon the GMWL.

Assuming constant temperature and elevation, this suggests a decrease in precipitation levels (Drever, 1997) since the deposition of the Siwalik sediments. For a quantitative estimate of the change in mean annual precipitation rate the township of Cherrapunji, located at the southern edge of the Shillong Plateau, receives an average precipitation of 11,000 mm/year in comparison to the Samdrup Jongkhar, which receives 5,300 mm/yr (Royal Government of Bhutan, 2012). The isotopic composition of meteoric water at Cherrapunji (2007-2008) (Breitenbach et al., 2010) is plotted in Figure 5.3 as an orange data point. It plots significantly closer to the isotopic composition of the Siwalik sediments than the eastern Bhutan present meteoric water. This comparison shows that the isotopic compositions of Siwalik sediments plot closer to Cherrapunji's, a region of significantly higher precipitation than that of eastern Bhutan.

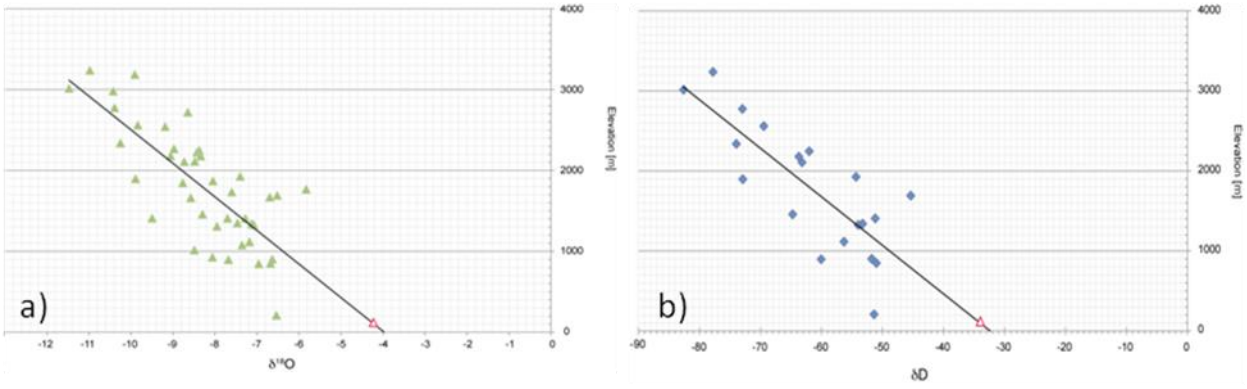

Figure 5.4: a) Elevation vs. $\delta^{18}O$ plot, showing the meteoric water isotopic compositions across eastern Bhutan in relation to their elevation. The scatter is due to changing latitudes of the samples. The $\delta^{18}O$ isotopic value at an elevation of 100 m is projected along the trend line. **b)** Elevation vs. δD plot, showing the meteoric water isotopic compositions across eastern Bhutan in relation to their elevation. The scatter is due to changing latitudes of the samples. The δD isotopic value at an elevation of 100 m is projected along the trend line.

5.4 GLOBAL CLIMATE CHANGES

There are four physical factors that can cause a change in $\delta^{18}O$ values: changes in temperature, latitude, elevation and precipitation (Dansgaard, 1964). When observing each of these factors independently while holding the others constant, the effect on the $\delta^{18}O$ values are shown in Table 5.1.

Table 5.1: Summary table of the impacts independent factors have upon the $\delta^{18}O$ values. Each factor is taken into consideration as the others are held constant.

Independent Factors	$\delta^{18}O$
Ice volume increase with global cooling	Increase in ‰
Precipitation decrease	Increase in ‰
Monsoon weakening (2.7-0 Ma)	Increase in ‰
Aridification	Increase in ‰
Northwards latitude shift by ~10˚	Decrease in ‰
Elevation Increase	Decrease in ‰
Monsoon intensification (7-8 Ma)	Decrease in ‰

The global paleoclimate record based on $\delta^{18}O$ compositions of carbonate-rich oozes and chalks shows an overall increase in $\delta^{18}O$ from the Middle Miocene to the Pliocene (Fig. 5.5) (Zachos et al., 2001). This increase in $\delta^{18}O$, within the oceans, corresponds to a global cooling period and increases in ice volume. When compared to the $\delta^{18}O$ record from this study, the global decrease in temperature, and increase in $\delta^{18}O$ of 2.5‰ could account for some of the 3.2‰ increase observed in the $\delta^{18}O$ values from the Siwalik deposition to present meteoric water.

Latitudinal changes of an area (sedimentary basin) due to the movement of crustal plates can cause $\delta^{18}O$ changes (Drever, 1997). $\delta^{18}O$ values range across the globe with varying latitudes, and in general $\delta^{18}O$ decreases with increasing latitude (Fig. 5.6) (Drever, 1997). India is known to have moved northward ~10° - 15° over the past 50 Ma (Quade et al., 2011). If this is the case, the $\delta^{18}O$ value from the time of deposition to present would have decreased by approximately 5‰ depending on the amount of plate motion, as the location moved further north, making the present day value lighter.

The $\delta^{18}O$ value of meteoric water decreases with increasing elevation (Drever, 1997; Quade et al., 2011). The latitudinal changes in $\delta^{18}O$ and also the changes in $\delta^{18}O$ due to elevation can be observed when comparing the lower $\delta^{18}O$ values of the Tibetan Plateau and Himalaya to the foreland basin values (Fig. 5.6). In this study the elevation of the Siwalik sedimentary basin could not have been different than the recent (i.e. Brahmaputra) foreland basin, i.e. ~ 100 m.

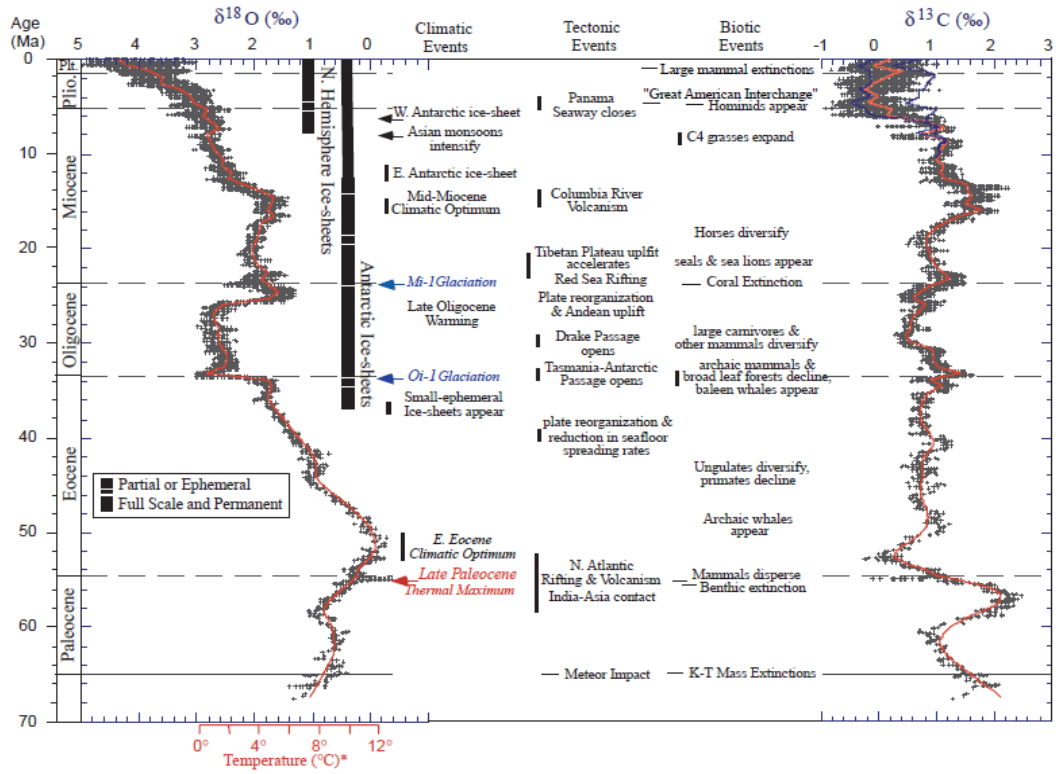

Figure 5.5: The global deep-sea oxygen and carbon isotope records from fine-grained, carbonate-rich (>50%) oozes or chalks. The isotopic compositions are given in ‰ PDB alongside their ages, and recorded climatic events, tectonic events and biotic events. The $\delta^{18}O$ plot also shows the calculated temperature for an ice-free ocean and therefore only applies to the time before the onset of large-scale glaciations on Antarctica (~35 Ma). From Zachos et al. (2001).

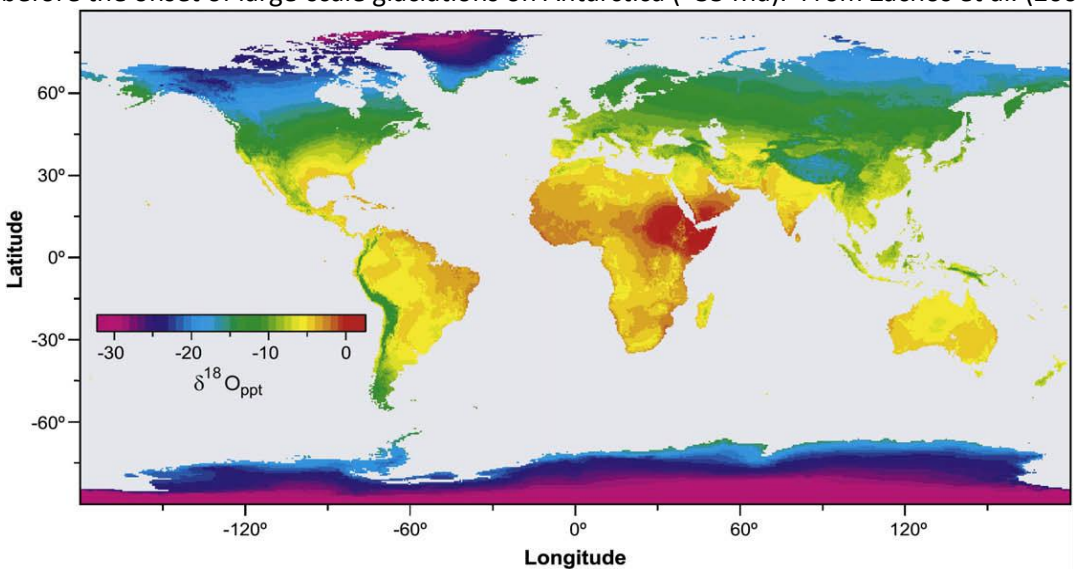

Figure 5.6: Global distribution of mean annual $\delta^{18}O$ showing the spatial distribution. In general, $\delta^{18}O$ values decrease from low to high latitudes and from low to high altitudes. From Lachniet et al. (2009).

The last factor to consider is precipitation and its affect on $\delta^{18}O$ values, also known as the "amount effect" (Dansgaard, 1964). The higher the precipitation levels, the lighter the $\delta^{18}O$ values become (Hoefs, 2009). If all other factors were held constant (temperature, latitude and elevation) and precipitation decreased, than the $\delta^{18}O$ value of the meteoric water would increase, since the heavier isotopes would be rained out preferentially and not diluted by lighter isotopes.

The period of intensification of the monsoon at approximately 7-8 Ma (Quade et al., 1989) would have caused a decrease in $\delta^{18}O$ values of the meteoric water within the regions affected by the monsoon due to the higher levels of precipitation. In contrast from 2.7 Ma until recent, the monsoon has weakened due to the global cooling event, thereby increasing the $\delta^{18}O$ values for meteoric water. As the global ice volumes increased, the ISM was affected by aridification, such that the strength decreased and more evaporation of the land ensued (Thomas et al., 2002). With high evaporation rates within the soils, the $\delta^{18}O$ values within the water become progressively heavier as the lighter isotopes are evaporated (Hoefs, 2009). Therefore, since 2.7 Ma there has been an overall increase in $\delta^{18}O$ values due to the global cooling event.

As there are four principal factors that affect the isotopic composition of the meteoric water, it would be difficult to pin one down as the cause of the 3.2 ‰ increase in $\delta^{18}O$ since the deposition of the Siwalik. However, some factors have been inferred to have less effect upon the study region. Modelling of the $\delta^{18}O$ values of meteoric water for New Delhi (to the west of Bhutan and also affected by the ISM), taking into account the opposite effects of the northward drift, and a decrease in soil temperature of ~14 °C due to the increasing global ice volume (Fig. 5.7), showed that the $\delta^{18}O$ value of New Delhi rainfall has remained constant over the past 50 Ma (Quade et al., 2011). The latitude and temperature effects would balance out. In conclusion, since eastern Bhutan's foreland basin's elevation has remained constant at 100 m, the only factor left to have changed since the Miocene is the precipitation.

There is no systematic observation of the "amount effect" and the two known studies yield inconsistent results (Lachniet et al., 2006; Breitenbach et al.,

2010). The record of mean monthly precipitation and isotopic composition of rain waters in New Delhi (Rowley et al., 2007) suggest that a change of 100 mm/month in precipitation corresponds to a change of 3.05 ± 0.15‰ $\delta^{18}O$. This is a similar value to 2.85 ‰/ 100 mm/ month obtained for Panama City (Lachniet et al., 2006). Breitenbach et al. (2011) however did not find a correlation amount per change in isotopic composition in Cherrapunji, but their observations cover a shorter time frame. The isotopic compositions of the Siwalik Group are interpreted to show an increase of 3.2‰ $\delta^{18}O$ since the deposition to Recent. For the qualitative interpretation of this observation I make the following assumptions: the clay minerals are all authigenic; the mean isotopic composition of the meteoric water in equilibrium with the Siwalik clay samples is correct; the composition of the meteoric waters within the eastern Bhutan Himalayas is correct; and the elevation and temperature have remained constant. In this case the increase in $\delta^{18}O$ could correspond to 100 mm/month, i.e., ~ 1200 mm/yr decrease in mean annual precipitation since the deposition of the Siwalik Group. This would only be true if the precipitation factor was the only factor causing the change in $\delta^{18}O$. This decrease in mean annual precipitation holds true to the working hypothesis, that eastern Bhutan has been receiving less precipitation since the Shillong Plateau uplifted at the Miocene-Pliocene boundary causing a strong orographic precipitation in the front and rain shadow in the lee. The Shillong Plateau is not the only factor affecting the change in precipitation distribution, as the global cooling and consequential weakening of the monsoon could also account for a portion of the decrease in precipitation and increase in $\delta^{18}O$.

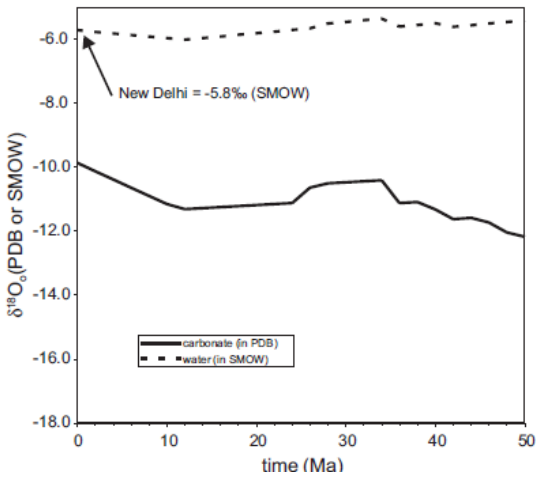

Figure 5.7: The modelled evolution of the $\delta^{18}O$ value for rainfall (in SMOW) in New Delhi through time compared to the $\delta^{18}O$ value from soil carbonates (in PDB). This model assumes a ~14 °C decrease in soil temperature, a 10° northward drift of India, and an ~1‰ in $\delta^{18}O$ value of seawater due to the increasing global ice volume. From Quade et al. (2011).

CHAPTER VI: CONCLUSION

6.1 SUMMARY

The preliminary XRD analyses of clay fractions from paleosols in foreland sediments of eastern Bhutan show the samples mainly contain clay minerals rather than detrital hydrous phyllosilicates (eg. muscovite). Suggestions for further research to determine whether or not these clay minerals are in fact authigenic or detrital are made at the end of this thesis.

Different techniques suggest different temperatures of paleo-meteoric waters. Clay isotopic compositions compared to qualitative kaolinite water lines suggest ~40 °C. The vitrinite reflectance data shows the maximum burial temperature of the Siwalik sediments to be 60± 10 °C. Smectite thermometry suggests 60 °C . The average annual temperature of the Himalayan foreland is 25 °C and is assumed to have stayed constant. Therefore the temperature window for which the clay minerals could have equilibrated with meteoric waters range from 25-60 °C. The mean meteoric water isotopic composition was calculated from the clay samples using the isotope fractionation factor between meteoric water and different clay minerals for temperatures between 20- 60 °C, which falls upon the eastern Bhutan water line for 50 °C. The so determined mean paleo-water isotopic composition, -7.4‰ $\delta^{18}O$, -56.8‰ δD compared to present meteoric water values at the same elevation (100 m), provides a difference of +3.2‰ $\delta^{18}O$.

The global paleoclimate record shows an overall decrease in temperature since the Middle Miocene, which would effectively weaken the monsoon and increase evaporation within the soil thereby increasing the $\delta^{18}O$ value since the Miocene. At the same time the northward propagation of India has led to a 10° latitude change over 50 Ma, and would decrease the $\delta^{18}O$ value since the Miocene. However Quade et al. (2011) inferred from modelling that the meteoric water isotopic composition in the foreland of the Himalaya has remained constant for the past 50 Ma, taking into account the latitudinal shift and a temperature decrease of approximately 14 °C. This observation therefore leaves elevation and precipitation as the factors affecting the change in $\delta^{18}O$ in eastern

Bhutan. As it is known that the elevation of the Siwalik samples has not changed, precipitation or the "amount effect" remains the only unknown physical factor for the change in $\delta^{18}O$. The available data suggested that 100 mm/month change in precipitation corresponds to a change of ~3‰ $\delta^{18}O$, such that the increase of 3.2‰ $\delta^{18}O$ since the Siwalik deposition would then correspond to a 1200 mm/yr decrease in mean annual precipitation. Though other factors could have affected the precipitation distribution in eastern Bhutan, the uplift of the Shillong Plateau seems to be the controlling factor. Since the Miocene-Pliocene transition a strong orographic precipitation resulted at the front of the Shillong Plateau causing a decrease of precipitation in the lee, such that eastern Bhutan receives significantly less precipitation today than during the deposition of the Siwalik Group. This would likely have changed the erosion rates in the foothills of the eastern Himalaya.

6.2 FURTHER RESEARCH

The primary scope of this study was to separate the clay minerals and determine their isotopic composition. The determination of clay composition was secondary although through the study it became evident that the more precise clay mineral identification and semi quantitative composition of the samples is important for the reliable interpretation of the isotopic data. However due to time constraints the additional clay analyses were not preformed.

The mineralogy of the clay minerals can be further constrained with further methods undertaken to properly analyze the clay minerals and distinguish them from one another. These would include methods of comparison between air-dried and ethylene glycol-solvated prepared samples (Moore, et al., 1997). For further methods of distinction between specific minerals refer to Chapter 3. Obtaining these data would allow for more quantitative analysis of the abundance of the clay minerals. As well, illite crystallinity can be used as a method of identifying detrital clay minerals (Huyghe et al., 2011). Since Illite can form from weathering, diagenesis or metamorphism, for this study it is important to determine which of these three processes formed the illite observed in the samples. Illite crystallinity is used to determine the diagenetic or low

metamorphic grade of sedimentary rocks using the Kübler Index (Huyghe et al., 2011). High crystallinity is attributed to the re-crystallization and transformation with increasing burial depth for smectite, illite-smectite mixed-layers and illite, where the final phase is muscovite (Huyghe et al., 2011). If the samples are analyzed and determined to have crystallinity temperate greater than 60 ˚C (the maximum burial temperature from vitrinite reflectance analysis) than the illite is dominantly detrital and vice versa.

The temperature change within eastern Bhutan from the Miocene to present would constrain the temperature of equilibration with meteoric waters. This would aid in the interpretation of the data, to determine whether the change in $\delta^{18}O$ is due primarily to precipitation changes, or whether temperature change was large enough to cause a perturbation in the $\delta^{18}O$ record. The temperature change through time could be determined through clumped isotope temperature analysis or δD analysis of individual leaf wax biomarkers (Hren et al., 2010), a study currently underway by Dr. Michael Hren, University of Tennessee.

The depositional ages are currently being analyzed by magnetostratigraphy. At the same time as the paleosol sampling, 224 drill cores were taken for magnetostratigraphy. The samples were measured by Dr. Guillaume Dupont-Nivet at the University Rennes, France. However the results are inconclusive and reference ages are needed. Tuff layers which are usually dated in the continental sediments are lacking in the study section. Instead, iodine ^{129}I dating from leaf matter could determine the depositional age of several leaf beds (Lu et al., 2011). The test sample is currently being measured by Dr. Liam Kieser at the IsoTrace Laboratory, University of Toronto. With the known stratigraphic age, the samples can quantitatively be compared with the global paleoclimate record and to the timing of the uplift of the Shillong Plateau. The ages of the sediments would also help to determine the sedimentation rates throughout the Siwalik deposition for comparison with the temporal variations of erosional rates to be determined by detrital thermochronology by Dr. I. Coutand at Dalhousie University. The eventual objective of these studies would be to determine more precisely the relationship between the changes of precipitation and changes in erosion and sedimentation.

REFERENCES

Baertschi, P. (1976). Absolute 18O content of standard mean ocean water. *Earth and Planetary Science Letters,* 31, 341-344.

Beaumont, C. (1981). Foreland basins. *Geophysical Journal of the Royal Astronomical Society*, 65, 291-329.

Bernet, M., Van der Beek, P., Pik, R., Huyghe, P., Mugnier, J-L., Labrin, E. & Szulcs, A. (2006). Miocene to Recent exhumation of the central Himalaya determined from combined detrital zircon fission-track and U/Pb analysis of Siwalik sediments, western Nepal. *Basin Research*, 18, 393-412.

Bilham, R. & England, P. (2001). Plateau Pop-up during the 1897 Assam earthquake. *Nature,* 410, 806-809.

Bilham, R., Bendick, R. & Wallace, K. (2003). Flexure of the Indian plate and intraplate earthquakes. *Proc. Indian Acad. Sci. Earth Planetary Science*, 112, 3, 315-329.

Biswas, S., Coutand, I., Grujic, D., Hager, C., Stockli, D. & Grademann, B. (2007). Exhumation and uplift of the Shillong plateau and its influence on the eastern Himalayas: New constraints from apatite and zircon (U-Th-[Sm])/He and apatite fission track analyses. *Tectonics*, 26, TC6013, doi:10.1029/2007TC002125.

Bookhagen, B. & Burbank, D.W. (2006). Topography, relief, and TRMM-derived rainfall variations along the Himalaya. *Geophysical Research Letters*, 33, L08405, doi: 10.1029/2006GL026037.

Bookhagen, B. & Burbank, D.W. (2010). Toward a complete Himalayan hydrological budget: Spatiotemporal distribution of snowmelt and rainfall and their impact on river discharge. *Journal of Geophysical Research*, 115. doi: 10.1029/2009JK001426.

Breitenbach, S.F.M., Adkins, J.F., Meyer, H., Marwan, N., Kumar, K.K., & Haug, G.H. (2010). Strong influence of water vapour source dynamics on stable isotopes in precipitation observed in Southern Meghalaya, NE India. *Earth and Planetary Science Letters*, 292 (1-2), 212-220.

Burbank, D.W., Beck, R.A. & Mulder, T. (1996). The Himalayan Foreland. In: Asian Tectonics (Ed. by Y. An & M. Harrison), pp. 149-188. Cambridge Univ. Press, Cambridge, MA.

Carlton College: Scientific Education Resource Center. Geochemical Instrumentation and Analysis: X-ray reflection in accordance with Bragg's Law. <http://serc.carleton.edu/research_education/geochemsheets/BraggsLaw.html > December 18, 2011.

Clark, M.K., & Bilham, R. (2008). Miocene rise of the Shillong Plateau and the beginning of the end for the Eastern Himalaya. *Earth and Planetary Science Letters*, 269, 337-351.

Clemens, S., Prell, W., Murray, D., Shimmield, G. & Weedon, G. (1991). Forcing mechanisms of the Indian Ocean monsoon. *Nature*, 353, 720-725, doi: 10.1038/353720a0.

Clift, P.D., Hodges, K.V., Heslop, D., Hannigan, R., Van Long, H., & Calves, G. (2008). Correlation of Himalayan exhumation rates and Asian Monsoon intensity. *Nature Geoscience*, 1. 875-880.

Columbia University: Environmental Health and Safety. 2009. X-ray Diffraction Machines: Uses and Hazards. <http://ehs.columbia.edu/News%20Letter/FA09Page4.html> December 18, 2011.

Dansgaard, W. 1964. Stable Isotopes in Precipitation. *Tellus*, 14, (4): 436-468.

DeCelles, P.G., Gehrels, G.E., Quade, J. & Ojha, T.P. (1998). Eocene-early Miocene foreland basin development and the history of Himalayan thrusting, western and central Nepal. *Tectonics*, 17, 5, 741-765.

DeCelles, P.G., Gehrels, G.E., Quade, J., Ojha, T.P., Kapp, P.A. & Upreti, B.N. (1998). Neogene forland basin deposits, erosional unroofing, and the kinematic history of the Himalayan fold-thrust belt, western Nepal. *Geological Survey of America Bulletin*, 110, 1, 2-21.

Delgado, A. & Reyes, E. (1996). Oxygen and hydrogen isotope composition in clay minerals: A potential single-mineral geothermometer. *Geochimica et Cosmochimica Acta*, 60, 21, 4285-4289.

Dettman, D.L., Kohn, M.J., Quade, J., Ryerson, F.J., Ojha, T.P. & Hamidullah, S. (2001). Seasonal stable isotope evidence for a strong Asian monsoon throughout the past 10.7 m.y. *Geology*, 29, 1, 31-34.

Dettman, D.L., Fang, X., Garzione, C.N. & Li, J. (2003). Uplift-driven climate change at 12 Ma: a long $\delta^{18}O$ record from the NE margin of the Tibetan plateau. *Earth and Planetary Science Letters*, 214, 267-277.

Drever, J.I. 1997. The Geochemistry of Natural Waters: Surface and Groundwater Environments. Prentice Hall, New Jersey. 311-321.

Ganju, P.N., & Srivastava, V.K. (1962). Occurrence of Greywacke in the Lower Siwaliks, Simla Hills. *Nature*, 194, 566-567, doi: 10.1038/194566b0.

Gansser, A. (1983). *Geology of the Bhutan Himalaya*: DSNG: Memoires de la Societe Helvetique des Sciences Naturelles, pp. 16-20, Basel: Birkhauser Verlag. Band Vol. 96.

Grujic, D., Coutand, I., Bookhagen, B., Bonnet, S., Blythe, A. & Duncan, C. (2006). Climatic forcing of erosion, landscape, and tectonics in the Bhutan Himalayas. *Geology*, 34, 10, 801-804.

Grujic, D., Warren, C.J., Wooden, J. (2011) Rapid synconvergent exhumation of Miocene-aged lower oro - genic crust in the Eastern Himalaya. *Lithosphere,* v. 3; no. 5; 346-366. doi: 10.1130/L154.1

Hagemann, R., Nief, G. & Roth, E. (1970). Absolute isotopic scale for deuterium analysis of natural waters. Absolute D/H ratio for SMOW. *Tellus*, 22, 712-715, doi: 10.1111/j.2153-3490.1970.tb00540.x.

Hodges, K. V., Parrish, R.R. and Searle, M.P., 1996, Tectonic evolution of the central Annapurna Range, Nepalese Himalayas. *Tectonics*, v. 15, no. 6, 1264-1291.

Hodges, K.V., 2000, Tectonics of the Himalaya and southern Tibet from two perspectives. *Geological Survey of America Bulletin*, v. 112, no. 3, 324-350.

Hoefs, J., 2009. *Stable Isotope Geochemistry: Sixth Edition*. Springer, Berlin. 19-181.

Hren, M.T., Pagani, M., Erwin, D.M. & Brandon, M. (2010). Biomarker reconstruction of the early Eocene paleotopography and paleoclimate of the northern Sierra Nevada. *Geology,* 38, 7-10, doi: 10.1130/G30215.1.

Huyghe, P., Galy, A., Mugnier, J-L., & France-Lanord, C. (2001). Propagation of the thrust system and erosion in the Lesser Himalaya: Geochemical and sedimentological evidence. *Geology,* 29, 11, 1007-1010.

Huyghe, P., Mugnier, J-L., Gajurel, A.P., & Delcaillau, B. (2005). Tectonic and climatic control of the changes in the sedimentary record of the Karnali River section (Siwaliks of western Nepal). *The Island Arc,* 14, 311-327.

Huyghe, P., Guilbaud, R., Bernet, M., Galy, A., & Gajurel, A.P. (2011). Significance of the clay mineral distribution in fluvial sediments of the Neogene to Recent Himalayan Foreland Basin (west-central Nepal). *Basin Research*, 23, 332-345, doi: 10.1111/j.1365-2117.2010.00485.x.

Jouanne, F., Mugnier, J.L., Gamond, J.F., Le Fort, P., Pandey, M.R., Bollinger, L., Flouzat, M. & Avouac, J.P. (2004). *Geophysical Journal International,* 157, 1-14, doi: 10.1111/j.1365-246X.2004.02180.x.

Kellett, D.A. 2010. *Tectonic evolution of the South Tibetan detachment system, Bhutan Himalaya*. PhD Thesis. Dalhousie University, Halifax, pp. 214- 219.

Lachniet, M.S., & Patterson, W.P. (2006). Use of correlation and stepwise regression to evaluate physical controls on the stable isotope values of Panamanian rain and surface waters. *Journal of Hydrology*, 324, (1-4), 115-140.

Lakshminarayana, G. & Singh, B. (1995). *Siwalik Group, in The Bhutan Himalaya: A Geological Account Ed. Bhargava*. Geological Survey of India, Special Publication 39, 23-28.

Long, S.P., McQuarrie, N., Tobgay, T., Rose, C.V., Gehrels, G., & Grujic, D. (2011). Tectonostratigraphy of the Lesser Himalaya of Bhutan: Implications for the stratigraphic architecture of the northern Indian margin. *Geological Survey of America Bulletin*, 123, 1406-1426, doi: 10.1130/B30202.1

Lu, Z., Tomaru, H. & Fehn, U. (2011). Comparison of Iodine dates from mud volcanoes and gas hydrates occurrences: Relevance for the movement of fluids

and methane in active margins. *American Journal of Science*, 311, 632-650, doi: 10.2475/07.2011.03.

Meigs, A.J., Burbank, D.W. & Beck, R.A. (1995). Middle-late Miocene (>10 Ma) formation of the main boundary thrust in the western Himalaya. *Geology,* 23, 423-426.

Moore, D.M. & Reynolds, R.C. Jr., 1997. *X-Ray Diffraction and the Identification and Analysis of Clay Minerals: 2nd Edition*. Oxford University Press, New York. 204-226

Nagelschmidt, G. (1941). The identification of Clay Minerals by means of aggregate X-ray Diffraction Diagrams. *Journal of Scientific Instruments*, 18 (5), 100.

Najman, Y., Johnson, K., White, N., & Oliver, G. (2004). Evolution of the Himalayan foreland basin, NW India. *Basin Research,* 16, 1-24.

Najman, Y. (2006). The Detrital record of orogenesis: A review of approaches and techniques used in the HImalayan sedimentary basins. *Earth-Science Reviews,* 74, 1-72.

Nesse, W., 2000. *Introduction to Mineralogy*. Oxford University Press, New York. 162-168.

Ohsawa, M. (Ed.) (1991). Life zone ecology of the Bhutan Himalaya: II. *Laboratory of Ecology*, Chiba University, Japan. 249.

Ojha, T.P., Butler, R.F., DeCelles, P.G. & Quade, J. (2009). Magnetic polarity stratigraphy of the Neogene foreland basin deposits of Nepal. *Basin Research*, 21, 61-90.

Ojha, T.P., Butler, R.F., Quade, J., Decelles, P.G., Richards, D., Upreti, B.N. (March, 2000). Magnetic Polarity stratigraph of the Neogene Siwalik Group at Khutia Khola, far western Nepal. *Geological Survey of America Bulletin*, 112, 3, 424-434.

Overpeck, J., Anderson, D., Trumbore, S. & Prell, W. (1996). The southwest Indian Monsoon over the last 18 000 years. *Climate Dynamics*, 12, 213-225, doi: 10.1007/BF00211619.

Pang, H., He, Y., Zhang, Z., Lu, A., & Gu, J. (2004). The origin of summer monsoon rainfall at New Delhi by deuterium excess. *Hydrology and Earth System Sciences*, 8(1), 115-118.

Parkash, B., Sharma, R.P. & Roy, A.K. (1980). The Siwalik Group (Molasse)-Sediments shed by collision of Continental Plates. *Sedimentary Geology*, 25, 1-2, 127-159.

Quade, J., Cerling, T.E. & Bowman, J.R. (1989). Development of Asian Monsoon revealed by marked ecological shift during the latest Miocene in Northern Pakistan. *Nature*, 342, 163-166.

Quade, J., Cater, J.M.L., Ojha, T.P. & Harrison, T.M. (1995). Late Miocene environmental change in Nepal and the northern Indian subcontinent: Stable isotopic evidence from paleosols. *Geological Survey of America Bulletin*, 107, 12, 1381-1397.

Quade, J., Breecker, D.O., Daeron, M., & Eiler, J. (2011). The Paleoaltimetry of Tibet: an Isotopic Perspective. *American Journal of Science*, 311,77-115, doi: 10.2475/02.2011.01.

Rao, R.U.M., Rao, G.V. & Narain, H. (1976). Radio-active heat generation and heat flow in the Indian shield. *Earth and Planetary Science Letters, 30, 57-64.*

Rowley, D.B. & Garzione, C.N. (2007). Stable Isotope-Based Paleoaltimetry. *Annual Review Earth Planetary Science*, 35, 463-508, doi: 10.1146/annurev.earth.35.031306.140155

Royal Government of Bhutan, Gross National Happiness Commission Report. Samdrup Jongkhar Local Government 10th five year plan (2008-2013). <http://www.gnhc.gov.bt/wp-content/uploads/2011/10thplan/Sjongkhar.pdf>. February 24, 2012.

Rumble D. III. and Hoering T.C., 1994. Analysis of oxygen and sulfur isotope ratios in oxide and sulfide minerals by spot heating with a carbon dioxide laser in a fluorine atmosphrere. *Accounts of Chemical Research*, 27: 237-241.

Sharp, Z.D., Atudorei, V. & Durakiewicz, T., 2001. A Rapid Method for determination of hydrogen and oxygen isotope ratios from water and hydrous minerals. *Chemical Geology*, 178: 197-210.

Sheppard, S.M.F., & Gilg, H.A. (1996). Stable isotope geochemistry of clay minerals. *Clay Minerals*, 31 (1), 1-24.

Stern, L.A., Chamberlain, C.P., Reynolds, R.C., & Johnson, G.D. (1997). Oxygen isotope evidence of climate change from pedogenic clay minerals in the Himalayan molasse. *Geochimica et Cosmochimica Acta*, 61, 4, 731-744.

Thomas, J.V., Parkash, B. & Mohindra, R. (2002). Lithofacies and palaeosol analysis of the Middle and Upper Siwalki Groups (Plio-Pleistocene), Haripur-Kolar section, Himachal Pradesh, India. *Sedimentary Geology*, 150, 343-366.

Tripathi, C. (1986). Siwaliks of the Indian Subcontinent. *Journal of the Palaeontological Society of India*, 31, 1-8.

Zachos, J., Pagani, M., Sloan, L., Thomas, E., & Billups, K. (2001). Trends, Rhythms, and Aberrations in Global Climate 65 Ma to Present. *Science*, 292, 686-693.

Zahid, K. M. & Uddin, A. (2005). Influence of overpressure on formation velocity evaluation of Neogene strata from the eastern Bengal Basin, Bangladesh. *Journal of Asian Earth Science*, 25, 419-429.

APPENDIX A

SAMLE PREPARATION
Dry Crushing (Hammer)

Equipment
- Bagged sample
- Clean metal plate upon a clean counter
- Hammer
- Sample bags
- Permanent marker

Safety Equipment*
- Gloves
- Face mask (Particulate respirator)
- Headband earmuff protection

* Always wear the safety equipment when handling samples*
** Before each use all equipment must be thoroughly cleaned**

Place the bagged sample upon the metal plate, and hammer the sample with even force and minimal swinging action. Once the sample is pulverized to powder, or else smaller than 2mm, move the sample into a new labeled sample bag. Continue to thoroughly clean all the instruments.

Figure A1: Equipment for dry crushing

Figure A2: Hammering the sample within its sample bags.

Wet Crushing (Mortar and Pestle)

Equipment
- Yogurt container (Beaker)
- Silica mortar and pestle
- Deionized water (17.2 Ohm)
- Permanent marker
- Scooping utensil

First pour the dry sample into a clean yogurt container up to a

Figure A3: Equipment for wet crushing

height of approximately 1 inch. Add deionized water (17 Ohm), covering the sample. Label the yogurt container with the sample number. Leave the sample to soak overnight.
Using your scooping utensil, scoop up the larger sample pieces and put them into the mortar. Do this in small amounts and add some of the deionized water to it. If the samples are dry this form of crushing could damage them. Using the pestle apply slight force to the larger pieces until they break apart. After the sample should be quite sticky like clay. Pour it back into the yogurt container, and wash the last
particles back in with the spray bottle.
* Thoroughly clean all utensils after use*

Figure A4: Add soaked sample to mortar and pestle with deionized water.

Blending
Equipment
- Waring Industrial Blender
- Ultrasonic bath
- Deionized water
- Scoopula
- Pressurized air
- soaked and crushed sample

Figure A5: Equipment for blending the soaked sample.

* All equipment must be thoroughly cleaned and the Waring blender dried using the pressurized air before and after use*

After the sample has been crushed, stir the sample into suspension and pour into the Waring blender. Blend the sample on low setting for

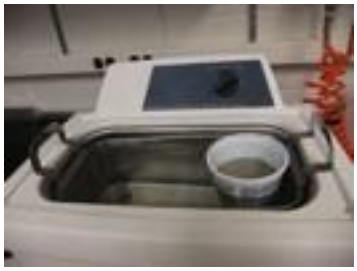

Figure A6: a) pouring the mixed sample into the Waring blender, **b)** place the sample in an ultrasonic bath for 5 minutes after blended.

approximately 4 minutes. Once the sample is in suspension pour it back into its yogurt container, using the spray bottle to get any sample off of the sides or bottom of the blender and back into the container. Turn the ultrasonic bath on and place the container in it, give the sample a few stirs with the scoopula, and then leave it there for 5 minutes. Once finished, put the lid back on and let it sit for 2 days. After 2 days most of the particles should have settled, decant the water so that there is only sample left.

Acetic Acid Treatment: Remove Carbonates

Equipment

- 50 mL vials made for the centrifuge
- Deionized water (17.2 Ohm)
- Glacial Acetic Acid
- Graduated Cylinder
- Stirring rods
- Permanent marker

Safety Equipment*

- Gloves
- Safety Glasses
- Lab Coat
- Fume Hood

Always wear safety equipment when handling acid

Thoroughly clean all equipment before and after use

Label the vials. Scrape 10 mL of sediment off of the top layer of the sample within the yogurt containers. Place within the labelled orange capped 50 mL vials. Measure

Figure A7: Equipment for Acetic Acid treatment.

Figure A8: a) 10 mL of sample put into centrifuge vials, **b)** 80 mL of deionized water with 20 mL of acetic acid to add to it in the fume hood..

out 4 parts deionized water to 1 part glacial acetic acid in the graduated cylinder within a fume hood. For this process, 80 mL of water was measured, and 20 mL of acetic acid was added. Stir this mixture. Add 25 mL of the acetic acid mixture to each sample and stir. Leave the samples in the fume hood for a few hours, and stir again.

Figure A9: Equipment for rinsing the samples of acetic acid with a centrifuge.

Once the samples have stopped effervescing, stir them up well, put their proper lids back on and place them in the centrifuge. Depending on how many the centrifuge will hold, is how many to treat with acetic acid at one time. Turn the centrifuge on at 2000 rpm for 5 minutes. Once the centrifuge is done, take the samples and decant the supernatant into an acetic acid waste beaker (labeled) to be disposed of properly. Continue rinsing out the sample by adding deionized water (approximately 25 mL) always to an equal value on the vials so that the centrifuge is balanced. Centrifuge another time for 5 minutes, and decant. Then centrifuge for 10 minutes for as many times as it takes to make the supernatant dusty looking. A total of 5-6 centrifuges may be needed to rinse the sample clean of the acetic acid.

Figure A10: After the first 5 minute centrifuge, decant the supernatant into a labelled acetic acid waste beaker.

Separation of <2 µm clay material: Centrifuge

Equipment

- Centrifuge
- Rinsed sample
- Stirring rods
- Ultrasonic bath
- Deionized water (17.2 Ohm)
- Clean centrifuge vials
- Permanent marker
- Disposable plastic pipettes
- Oven

Thoroughly clean all equipment before and after use.

Figure A11: Equipment for separation.

In order to determine the time and speed for centrifuging the sample a few variables are needed to determine the calculation for Equation 1 (Table 3.1; 3.2). From the equation in Figure 12, the time was determined to be 79 seconds. Therefore, including the time for acceleration, the samples are run for 1 minute and 43 seconds.

R_1= 6.8 cm

R_2 (to centre)= 9.2 cm

R_2 (to 10 mL)= 11.9 cm

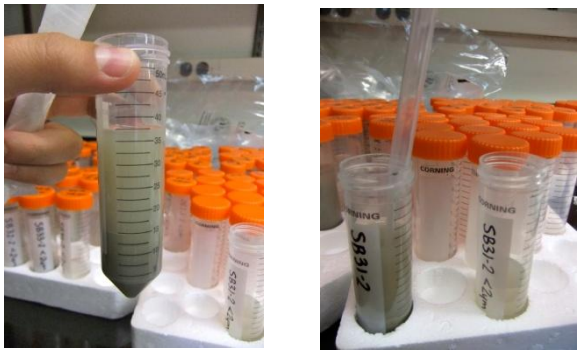

Figure A12: Decant the <2 um supernatant into a new labelled vial.

Add deionized water to the rinsed samples, approximately 25 mL. Stir the sample so that it is in suspension, close the lid and shake. Place the sample in an ultrasonic bath for 1-2 minutes to separate any flocculating particles. Put the samples in the centrifuge and turn the speed to 800 rpm. Centrifuge for a total of 103 seconds.

Decant the supernatant (using a pipette) into a clean centrifuge vial labeled with the sample number and "<2 µm." If the sample does not

provide enough material repeat the process. When finished fill the supernatant <2 μm vials with deionized water to balance the vials, and centrifuge them, to be sure that any larger particles are removed. Once the vial only contains < 2 μm particles, place the vials in an oven, at a temperature below 60 ˚C until dry. Once the sample is dry, scrape it off of the bottom and measure the amount of sample needed into a final vial.

Weighing samples

Equipment

- Balance
- Weighing paper
- Spatula
- Samples
- Vials
- Ethanol
- Kim Wipes

Figure A13: Equipment for weighing in the samples.

Using the Ethanol and Kim Wipes, clean the spatula. Cut the weighing paper to fit the balance.
Place the weighing paper upon the balance, close the side doors, Tare the scale. Using the Spatula place the dry sample upon the weighing paper. Close the side doors and record the weight.
For the oxygen and hydrogen analysis, the samples were weighed for a total of 30 mg.
Once weighed and recorded, take the weighing paper with sample and transfer the sample to a smaller carrying vial. Close the vial, and continue for the rest of the samples. Clean the spatula between uses, and always use a new weighing paper.

APPENDIX B

XRD analyses for each sample are on the CD as file: XRDanalysis.docx.

APPENDIX C

Original oxygen and hydrogen analyses results are on the attached CD as file: Oresults.xls, and Hresults.xls.

Table C1: Summary table of the GPS locations of the samples with their sample number, alongside the stratigraphic thickness and the clay isotopic data for $\delta^{18}O$, δD and D-excess in VSMOW. The calculated values of $\delta^{18}O$ and δD for water in equilibrium with the clay minerals from Equation 6 and 7 are shown for temperatures of 35 ˚C and 60 ˚C.

N°	E°	Sample #	Clay data	stratigraphic thickness [m]	Clay data	Clay data	Clay data	water 35 °C	water 35 °C	water 35 °C	water 60 °C	water 60 °C	water 60 °C
			Identifier		$\delta^{18}O$	δD	excess D	$\delta^{18}O$	δD	excess D	$\delta^{18}O$	δD	excess D
		SB4-2	SB04		12.07	-87.89	-184.43	-10.11	-57.03	23.85	-6.06	27.52	75.96
26.81	91.50	SB5-2	SB05		12.63	-97.76	-198.77	-9.55	-66.89	9.51	-5.50	54.33	98.30
		SB6-2	SB06		13.13	-95.74	-200.76	-9.05	-64.87	7.52	-4.99	27.52	67.48
26.81	91.50	SB7-2	SB07	15	12.12	-95.96	-192.88	-10.06	-65.09	15.40	-6.01	54.33	102.39
			SB07.25	15	12.22	-94.71	-192.46	-9.96	-63.85	15.82	-5.90	27.52	74.75
			SB07.5	15	12.62	-93.72	-194.64	-9.56	-62.86	13.64	-5.51	27.52	71.58
26.81	91.50	SB8-2	SB08	55	11.51	-98.64	-190.75	-10.66	-67.77	17.54	-6.61	54.33	107.21
26.81	91.50	SB9-2	SB09	70	12.37	-103.83	-202.81	-9.80	-72.97	5.47	-5.75	54.33	100.33
26.81	91.49	SB10-2	SB10	90	13.08	-100.94	-205.58	-9.10	-70.07	2.70	-5.04	54.33	94.67
26.81	91.49	SB11-2	SB11	115	12.50	-92.27	-192.29	-9.67	-61.40	15.99	-5.62	54.33	99.29
26.81	91.49	SB12-2	SB12	135	12.22	-90.11	-187.90	-9.95	-59.24	20.38	-5.90	54.33	101.51
26.81	91.49	SB13-2	SB13	155	11.83	-84.92	-179.56	-10.35	-54.05	28.72	-6.29	54.33	104.67
26.81	91.49	SB14-2	SB14	265	11.83	-86.00	-180.65	-10.35	-55.13	27.63	-6.29	54.33	104.66
		SB14B-2	SB14B	280	11.70	-91.39	-185.00	-10.48	-60.53	23.28	-6.42	27.52	78.89
26.81	91.49	SB15-2	SB15	315	11.88	-85.30	-180.38	-10.29	-54.44	27.90	-6.24	54.33	104.23
26.81	91.49	SB16-2	SB16	350	12.38	-83.33	-182.35	-9.80	-52.46	25.93	-5.74	54.33	100.29
26.81	91.49	SB17-2	SB17	360	12.21	-84.30	-181.99	-9.96	-53.43	26.29	-5.91	54.33	101.61
26.81	91.49	SB18-2	SB18	365	12.16	-85.18	-182.49	-10.01	-54.31	25.80	-5.96	54.33	102.01
26.81	91.49	SB20-2	SB20	375	12.54	-92.65	-192.95	-9.64	-61.78	15.33	-5.58	54.33	99.01
			SB21	380	12.41	-89.56	-188.80	-9.77	-58.69	19.49	-5.72	54.33	100.07
26.81	91.49	SB22-2	SB22	390	12.54	-85.24	-185.54	-9.64	-54.37	22.74	-5.59	54.33	99.01
26.81	91.49	SB23-2	SB23	440	12.69	-84.05	-185.55	-9.49	-53.18	22.73	-5.44	54.33	97.82
26.81	91.49	SB24-2	SB24	455	13.03	-82.64	-186.86	-9.15	-51.77	21.42	-5.09	54.33	95.09
26.81	91.49	SB25-2	SB25	470	12.67	-86.91	-188.31	-9.50	-56.04	19.98	-5.45	54.33	97.92
26.81	91.49	SB26-2	SB26	505	13.11	-86.27	-191.15	-9.07	-55.40	17.13	-5.01	54.33	94.43
26.81	91.49	SB27-2	SB27	508	12.76	-87.54	-189.59	-9.42	-56.67	18.69	-5.37	54.33	97.26
26.81	91.49	SB28-2	SB28	515	12.48	-85.62	-185.42	-9.70	-54.75	22.86	-5.65	54.33	99.51
26.81	91.49	SB29-2	SB29	530	12.34	-86.12	-184.85	-9.83	-55.25	23.43	-5.78	54.34	100.58
26.81	91.49	SB31-2	SB31	610	11.84	-86.82	-181.54	-10.34	-55.95	26.74	-6.28	54.34	104.59
26.82	91.49	SB32-2	SB32	625	12.66	-86.69	-187.96	-9.52	-55.82	20.32	-5.46	54.34	98.04
26.82	91.49	SB33-2	SB33	630	12.05	-88.63	-184.99	-10.13	-57.77	23.29	-6.08	54.34	102.96
26.82	91.49	SB34-2	SB34	635	12.34	-83.77	-182.46	-9.84	-52.90	25.82	-5.79	54.34	100.63
26.82	91.49	SB35-2	SB35	640	12.47	-86.21	-185.93	-9.71	-55.35	22.35	-5.66	54.34	99.60
26.82	91.49	SB36-2	SB36	650	11.80	-84.49	-178.86	-10.38	-53.62	29.42	-6.33	54.34	104.95

26.82	91.49	SB37-2	SB37	653	12.41	-84.86	-184.11	-9.77	-53.99	24.18	-5.72	54.34	100.07
26.82	91.49	SB38-2	SB38	655	12.17	-82.96	-180.29	-10.01	-52.09	28.00	-5.96	54.34	101.99
26.82	91.49	SB39-2	SB39	665	12.24	-84.01	-181.91	-9.94	-53.14	26.37	-5.88	54.34	101.41
26.82	91.49	SB40-2	SB40	675	12.06	-81.45	-177.94	-10.12	-50.58	30.35	-6.06	54.34	102.83
26.82	91.49	SB42-2	SB42	695	11.93	-85.24	-180.69	-10.25	-54.37	27.59	-6.19	54.34	103.87
26.82	91.49	SB43-2	SB43	700	12.12	-89.25	-186.18	-10.06	-58.38	22.10	-6.01	54.34	102.38
26.82	91.49	SB44-2	SB44	710	12.51	-81.77	-181.82	-9.67	-50.90	26.46	-5.62	54.34	99.27
26.82	91.49	SB45-2	SB45	735	13.00	-83.93	-187.93	-9.18	-53.07	20.35	-5.12	54.34	95.32
26.82	91.49	SB46-2	SB46	738	12.19	-84.03	-181.57	-9.98	-53.17	26.71	-5.93	54.34	101.78
26.82	91.49	SB47-2	SB47	750	12.89	-84.68	-187.77	-9.29	-53.81	20.51	-5.24	54.34	96.23
26.82	91.49	SB48-2	SB48	805	12.47	-81.94	-181.74	-9.70	-51.08	26.55	-5.65	27.52	72.71
26.82	91.49		SB48.25	805	12.34	-83.43	-182.11	-9.84	-52.56	26.17	-5.79	27.52	73.82
26.82	91.49		SB48.5	805	12.21	-83.24	-180.89	-9.97	-52.37	27.39	-5.92	54.34	101.66
26.82	91.49	SB49-2	SB49	820	12.79	-84.39	-186.68	-9.39	-53.52	21.60	-5.34	54.34	97.02
26.82	91.49	SB50-2	SB50b	825	12.35	-85.66	-184.45	-9.83	-54.79	23.83	-5.77	54.34	100.53
26.82	91.49	SB51-2	SB51	835	12.08	-86.38	-183.00	-10.10	-55.51	25.29	-6.05	54.34	102.70
26.82	91.49	SB52-2	SB52	930	12.42	-83.32	-182.68	-9.76	-52.45	25.60	-5.70	54.34	99.96
26.82	91.48	SB53-2	SB53	960	12.41	-88.82	-188.13	-9.76	-57.95	20.15	-5.71	54.34	100.01
26.82	91.48	SB54-2	SB54	970	12.48	-83.58	-183.42	-9.70	-52.71	24.86	-5.64	54.34	99.48
26.82	91.48	SB55-2	SB55	1,035	11.92	-82.40	-177.74	-10.26	-51.53	30.54	-6.21	54.34	103.98
26.82	91.48	SB56-2	SB56	1,050	12.06	-82.18	-178.68	-10.11	-51.32	29.60	-6.06	54.34	102.82
26.82	91.48	SB57-2	SB57	1,060	11.96	-85.77	-181.47	-10.21	-54.90	26.81	-6.16	54.34	103.62
26.82	91.48	SB58-2	SB58	1,063	11.46	-87.02	-178.73	-10.71	-56.15	29.55	-6.66	54.34	107.61
26.82	91.48	SB59-2	SB59	1,068	12.57	-82.04	-182.58	-9.61	-51.17	25.70	-5.55	54.34	98.78
26.82	91.48	SB60-2	SB60	1,070	12.07	-84.55	-181.14	-10.10	-53.68	27.14	-6.05	54.34	102.72
26.82	91.48	SB61-2	SB61	1,075	12.09	-84.21	-180.91	-10.09	-53.34	27.38	-6.03	54.34	102.62
26.82	91.48	SB62-2	SB62	1,085	12.43	-82.36	-181.78	-9.75	-51.49	26.50	-5.69	54.34	99.90
26.82	91.48	SB63-2	SB63	1,095	12.28	-84.17	-182.38	-9.90	-53.30	25.90	-5.85	54.34	101.11
26.82	91.48	SB64-2	SB64	1,120	12.17	-85.70	-183.08	-10.00	-54.83	25.20	-5.95	54.34	101.94
26.82	91.48	SB65-2	SB65	1,140	12.46	-88.87	-188.54	-9.72	-58.00	19.74	-5.66	27.52	72.83
26.82	91.48		SB65.25	1,140	12.17	-96.19	-193.52	-10.01	-65.32	14.76	-5.96	27.52	75.17
26.82	91.48		SB65.5	1,140	12.61	-87.25	-188.09	-9.57	-56.38	20.19	-5.52	54.34	98.47
26.82	91.48	SB66-2	SB66	1,150	12.87	-86.50	-189.46	-9.31	-55.63	18.82	-5.25	54.34	96.36
26.82	91.48	SB67-2	SB67	1,155	12.51	-82.10	-182.21	-9.66	-51.24	26.07	-5.61	54.34	99.22
26.82	91.48	SB68-2	SB68	1,165	11.82	-84.00	-178.53	-10.36	-53.14	29.75	-6.31	54.34	104.79
26.82	91.48	SB69-2	SB69	1,185	12.44	-83.42	-182.95	-9.73	-52.55	25.33	-5.68	54.34	99.78
26.82	91.48	SB70-2	SB70	1,265	12.80	-84.19	-186.60	-9.38	-53.32	21.68	-5.32	54.34	96.91
26.82	91.48	SB71-2	SB71	1,280	12.92	-85.84	-189.22	-9.25	-54.97	19.06	-5.20	54.34	95.94
26.82	91.48	SB72-2	SB72	1,290	12.77	-86.53	-188.70	-9.40	-55.66	19.58	-5.35	54.34	97.14
26.82	91.48	SB73-2	SB73	1,310	12.41	-85.24	-184.53	-9.77	-54.37	23.75	-5.71	54.34	100.03
26.82	91.48	SB74-2	SB74	1,355	12.11	-89.00	-185.88	-10.07	-58.13	22.40	-6.01	54.35	102.44
26.83	91.47	SB77-2	SB77	1,815	13.31	-86.95	-193.43	-8.87	-56.08	14.85	-4.81	54.35	92.85
26.83	91.47	SB78-2	SB78	1,865	13.09	-90.02	-194.71	-9.09	-59.15	13.57	-5.04	54.35	94.64
26.83	91.47	SB80-2	SB80	2,080	12.33	-90.80	-189.42	-9.85	-59.93	18.86	-5.79	54.36	100.71
26.83	91.47	SB81-2	SB81	2,080	13.63	-84.43	-193.49	-8.54	-53.56	14.79	-4.49	54.36	90.27
26.83	91.47	SB82-2	SB82	2,085	13.37	-83.32	-190.30	-8.80	-52.45	17.98	-4.75	54.36	92.36
26.84	91.48	SB84-2	SB84	2,175	13.55	-83.05	-191.43	-8.63	-52.18	16.85	-4.58	27.52	64.12
26.84	91.48	SB85-2	SB85	2,185	14.25	-83.87	-197.90	-7.92	-53.01	10.38	-3.87	27.52	58.47

26.84	91.48		SB85.25	2,185	14.16	-84.79	-198.05	-8.02	-53.92	10.23	-3.96	54.36	86.07
26.84	91.48		SB85.5	2,185	14.28	-85.04	-199.29	-7.90	-54.17	8.99	-3.84	54.36	85.09
26.84	91.48	SB86-2	SB86	2,190	13.29	-85.08	-191.41	-8.88	-54.21	16.87	-4.83	54.36	93.00
26.84	91.48	SB86-2 +	SB86+	2,190	13.56	-88.25	-196.72	-8.62	-57.38	11.56	-4.56	54.36	90.86
26.84	91.48	SB86-2 -	SB86-	2,190	12.26	-87.08	-185.15	-9.92	-56.22	23.13	-5.86	54.36	101.27
26.84	91.48	SB87-1	SB87	2,205	14.26	-85.99	-200.08	-7.91	-55.12	8.20	-3.86	54.36	85.24

Table C2: Equation 9 was used to calculate these values to reproduce the GMWL within Figures 5.1 & 5.3.

GMWL - O	GMWL- D
-1	3.07
-2	-5.13
-3	-13.33
-4	-21.53
-5	-29.73
-6	-37.93
-7	-46.13
-8	-54.33
-9	-62.53
-10	-70.73
-11	-78.93
-12	-87.13
-13	-95.33
-14	-103.53
-15	-111.73
-16	-119.93
-17	-128.13
-18	-136.33
-19	-144.53
-20	-152.73

Table C3: Calculations for mean isotopic composition of meteoric water from the mean isotopic composition of the clay values (Equation 7 & 8).

Temperature (°C)	Fractionation Factor for $\delta^{18}O$	Fractionation Factor for δD	mean clay $\delta^{18}O$	Mean water $\delta^{18}O$	mean Clay δD	Mean Water δD
10	27.6752	-35.1403	12.3424	-15.3328	-85.5304	-50.3900
20	25.3666	-33.3002	12.3424	-13.0242	-85.5304	-52.2302
30	23.2827	-31.6391	12.3424	-10.9403	-85.5304	-53.8913
40	21.3952	-30.1346	12.3424	-9.0528	-85.5304	-55.3958
50	19.6802	-28.7676	12.3424	-7.3378	-85.5304	-56.7628
60	18.1173	-27.5218	12.3424	-5.7749	-85.5304	-58.0086
70	16.6891	-26.3833	12.3424	-4.3467	-85.5304	-59.1470
80	15.3805	-25.3402	12.3424	-3.0381	-85.5304	-60.1901
90	14.1784	-24.3821	12.3424	-1.8360	-85.5304	-61.1483